Studies on the Role of Surrogate Light Chain in Antibody Repertoire Formation

Lin SUN

January 2018

Studies on the Role of Surrogate Light Chain in

Antibody Repertoire Formation

A Dissertation Submitted to the Graduate School of Life and Environmental Sciences,
the University of Tsukuba in Partial Fulfillment of the Requirements
for the Degree of Doctor of Philosophy in Science
(Doctoral Program in Biological Sciences)

Lin SUN

Table of Contents

Abbreviations

Arg: arginine

CDR-3: complementarity determining region-3

FO: follicular

Ig: immunoglobulin

LC: light chain

μHC: μ heavy chain

MZ: marginal zone

NGS: next generation sequencer

pre-BCR: pre-B cell receptor

SLC: surrogate light chain

WT: wild-type

KO: knock-out

PC: plasma cell

MBC: memory B cell

Abstract

The pre-B cell receptor (pre-BCR), which consists of the μ heavy chain (μHC) and the surrogate light chain (SLC, Vpre-B and λ5), exerts important roles during B cell development. The formation of the pre-BCR, that assesses the ability of the nascent immunoglobulin HC to associate with the SLC, is considered a prerequisite for B cell development. However, a significant number of peripheral mature (leaky) B cells exist in SLC-deficient mice. These leaky B cells develop in the absence of pre-BCR and do not undergo the pre-BCR checkpoint. The antibody repertoires of leaky B cells thus reflect the absence of pre-BCR function. To investigate how the absence of the pre-BCR is circumvented by these leaky B cells and the effect of the pre-BCR checkpoint on the antibody system, I analyzed the antibody repertoires of λ5-deficient ($λ5^{-/-}$) mice using next generation sequencing. In $λ5^{-/-}$ mice, spleen B cells displayed different patterns of VDJ-usage, relative to those in wild-type (WT) mice. Moreover, leaky B cells were neither derived from unusual B2 cells, characterized by particular LC gene rearrangements in the absence of pre-BCR signaling, nor from B1 cells, originating from different B cell progenitors. By analyzing the CDR-H3 amino acid sequences of μ-chain repertoires, I observed that certain bone marrow B cells with particular CDR-H3 profiles undergo clonal expansion in $λ5^{-/-}$ mice. Parts of these CDR-H3s contain arginine(s) in the middle of the CDR-H3 loop in $λ5^{-/-}$ mice, whereas few arginine(s) exist in this middle

loop in WT CDR-H3s in the absence of clonal expansion. This CDR-H3 feature in $\lambda 5^{-/-}$ mice presumably reflects the role of the pre-BCR in autoantibody regulation, since arginine(s) are often found in the antigen-binding site of autoantibodies. I present a unique viewpoint on the role of pre-BCR, by assessing the whole antibody repertoire formed in SLC-deficient mice.

General Introduction

The recognition of antigens by antibodies represents one of the fundamental processes of biological defense in vertebrates. Antibody-producing B cells develop in the bone marrow under various regulatory cues and form the repertoire of antigen-specific B cell clones (Melchers 2015). The size of the antibody repertoire was calculated as 10^{15} (Schroeder 2006), which is too big to capture using preexisting immunological methods. However, the recent advent of next generation sequencing (NGS) achieved a breakthrough in the study of antibody repertoires (Weinstein, Jiang et al. 2009, Georgiou, Ippolito et al. 2014). Moreover, my group has recently reported a simple method for visualizing the holistic view of mouse antibody repertoire dynamics using NGS (Kono, Sun et al. 2017).

B cells develop in the bone marrow, giving rise to a repertoire of antigen-specific clones, and undergo a major differentiation checkpoint, mediated by the pre-B cell receptor (pre-BCR) (Melchers 2015). The pre-BCR is composed of the immunoglobulin µ heavy chain (Ig-µHC) and the surrogate light chain (SLC), containing Vpre-B and λ5, and allows for the progression of differentiation only in B cell precursors that have successfully undergone recombination at the IgH gene locus (Karasuyama, Kudo et al. 1990, Tsubata and Reth 1990). At this stage of development, the newly produced IgH assembles with the invariant SLC to form the pre-BCR, where the association with the

SLC serves as a quality check for IgH (Karasuyama, Rolink et al. 1994, Melchers 2005). The formation of the pre-BCR assesses not only the productivity of the nascent IgH, but also its autoreactivity (Keenan, De Riva et al. 2008, Herzog and Jumaa 2012, Melchers 2015).

$\lambda 5^{-/-}$ mice are phenotypically similar to those lacking Vpre-B or the entire SLC (Kitamura, Kudo et al. 1992, Shimizu, Mundt et al. 2002), characterized by severe impairments in B cell development. However, this accompanies the characteristic generation of a significant number of mature B cells (leaky B cells). These leaky B cells develop in the absence of pre-BCR, implying that the repertoire of leaky B cells reflects the function of pre-BCR checkpoint.

To explore the role of pre-BCR in antibody formation, I used NGS to compare the full antibody repertoires of wild-type (+/+, WT) and $\lambda 5^{-/-}$ mouse littermates. The expansion of bone marrow B cells in $\lambda 5^{-/-}$ mice displayed characteristic repertoire patterns, suggesting a specific role for CDR-H3 sequences in the formation of antibody repertoires. My approach uniquely addresses pre-BCR function in this context.

Chapter 1

Deciphering Antibody Repertoires with Next Generation Sequencing

Introduction

The antibody-producing B cell repertoire is generated by VDJ gene recombination. During early B cell development, productive Ig-μHC rearrangement is monitored by deposition of the Ig-μHC protein on the cell surface, together with SLC as the pre-BCR complex. The first checkpoint is exerted by pre-BCR expression that monitors for functional IgHC rearrangement. Subsequently, the pre-BCR triggers proliferative expansion and represents the second major checkpoint, the rearrangement for Ig-μHC with Igκ or Igλ LC loci. The theoretical value of the antibody repertoire in mice is estimated to be 10^{15}, however, the actual value of generated B-cell repertoires is estimated to be $10^{8\sim9}$ in an individual. This astronomical number of B-cell clones has been regarded as a "black-box".

Here, I used next generation sequencing (NGS) to analyze the deep profiles of antibody repertoires. In order to obtain a global view of the common and unique features of antibody repertoires generated in individual mice, my group developed a simple and confirmative method to decipher antibody repertoires. At first, I analyzed the sequences of antibody transcripts for the naive mice, and the mice immunized with the model antigen, nitrophenol (NP)-hapten linked to chicken γ-globulin (CGG) carrier. By comparing holistic aspects of B-cell repertoires of individual mice, common usage of

IGHV1-72/IGHD1-1/IGHJ2 for NP and IGHV9-3/IGHD3-1/IGHJ2 for CGG-carrier protein were detected. The IGHV1-72, also known as Vh186.2, is a widely recognized anti-NP antibody in C57BL/6 mice (Cumano and Rajewsky 1985, Furukawa, Akasako-Furukawa et al. 1999). The consistency of result on NP-specific antibody repertories proved the availability of this prediction protocol. Moreover, I synthesized the VDJ sequences of detected antibody genes that was selected from NGS-output reads, and checked their antigen-binding activity.

Besides, I tried MiSeq system to check if it is more superior to obtain the raw reads comparing to highthroughput pyrosequencing (Roche) 454 system. For the same sample, approximately 10^6 of reads for one NGS run were collected by using MiSeq system as compared to approximately 10^4 reads by using Roche 454 system.

In this study, I obtained a global view of antibody repertoires by using NGS. And with the method developed by my group, common antigen-responding antibody repertoires were obtained by comparing holistic aspects of B-cell repertoires of individual mice. And by the improvement of sequencing system，approximately 10^6 of reads for one NGS run were able to be obtained for analyzing the global view of antibody repertoires.

Materials and Methods

Mice and ethics statements

The λ5 gene targeted mice, λ5-deficient ($\lambda5^{-/-}$) mice (Kitamura, Kudo et al. 1992) was backcrossed more than 10 generations to the C57BL/6 background, and maintained in specific-pathogen-free (SPF) conditions. WT and $\lambda5^{-/-}$ homozygous littermates were used throughout all experiments. All animal experiments were performed according to the institutional guidelines and with the approval of the National Institute of Infectious Diseases Animal Care and Use Committee (Permit Number: 213045-2).

Mice were housed under a 12-hour light/dark cycle, and provided with food and water ad libitum. Mice were euthanized by carbon dioxide inhalation and the spleens were explanted.

RNA preparation and cDNA synthesis

Spleen, bone marrow tissues or sorted spleen B cells are homogenized in the presence of the TRIZOL (Thermofisher, Cat. 15596-018) to permit dissociation of the nucleoproteins complex, and subsequently add chloroform for lysis. RNA was isolated using PureLink RNA Mini Kit (Ambion, 12183018A). Two to 10 μg of total RNA was reversely transcribed using SMARTer® RACE 5'/3' Kit (Clontech Laboratories, 634860).

Next, cDNA were ampurified by PCR in a 20μl reaction mixture according to institutional

guidelines (Figure 1).

PCR amplification in Roche 454 pyrosequencing system

Universal forward primers of 5'-RACE containing Multiplex Identifier (MID) adaptors

(MID9_NUP 5 '-TAGTATCAGCAAGCAGTGGTATCAACGCAGAGT-3', MID11_N-

UP 5'-TGATACGTCTAAGCAGTGGTATCAACGCAGAGT-3', MID14_NUP 5'-CGA-

GAGATACAAGCAGTGGTATCAACGCAGAGT-3') were used with reverse primers

specific for IgM primer (5'-CACCAGATTCTTATCAGACAGGGGGCTCTC-3') to

amplify IgM repertoires through thermal cycling (98 ˚C for 30 sec, 40 cycles of 98 ˚C for

10 sec, 71 ˚C for 15 sec, 72 ˚C for 30 sec, and a final extension at 72 ˚C for 5 min). The

600-800 bp PCR products were gel purified using Wizard® SV Gel and PCR Clean-Up

System (Promega, A9282). The purified PCR products were analyzed by Roche 454

pyrosequencing system.

PCR amplification in MiSeq system

cDNA was amplified with Taq DNA polymerase (TaKaRa RR006A) as follows.

Universal forward primers 5'-AAGCAGTGGTATCAACGCAGAGT was used with the

reverse primes specific for IgM primer 5'- CACCAGATTCTTATCAGACAGGGGGCT-CTC-3', IgG1primer 5'- CATCCCAGGGTCACCATGGAGTTAGTTTGG-3', IgG2c primer 5'- GTACCTCCACACACAGGGGCCAGTGGATAG-3', Igκ primer 5'-GCTC-ACTGGATGGTGGGAAGATGGATACAG-3' and Igλ primer 5'-CTBGAGCTCYTCA-GRGGAAGGTGGAAACA-3' to amplify the repertoires of each isotype by the thermal cycling; 94 ˚C for 2 min, 20 cycles of 94 ˚C for 30 sec, 59 ˚C for 30 sec, 72 ˚C for 30 sec, followed by a final 72 ˚C 5 min extension step. The PCR products were re-amplified by using the primer pair from FASMAC Co., Ltd. with the same thermal cycling condition of 40 cycles. The 600-800 bp PCR products were purified using Wizard® SV Gel and PCR Clean-Up System (Promega, A9282). The purified PCR products were analyzed by MiSeq system (FASMAC Co., Ltd.).

Visualization of the V(D)J repertoires

The raw reads obtained by MiSeq system were quality-checked and filtered for more than 200bp-long. The pipeline for antibody sequence analysis was described previously (Kono, Sun et al. 2017). Briefly, read sequences were classified into antibody classes by searching for the class-specific CH1 sequence. The V_H, J_H, D_H and V_L, J_L genes were annotated by using standalone IgBlast program. IgH repertoires were visualized by the

array on the three-dimensional mesh in which x-axis represents 110 x IGHV genes, y-axis represents 12 x IGHD genes and z-axis represents 4 x IGHJ genes, and IgL were visualized by the array on the two-dimensional diagram in which x-axis represents 110 x IGLVκ and 4 x IGLVλ genes, y-axis represents 4 x IGLJκ and 4 x IGLJλ genes. The volume of each sphere on IGH gene represents the number of reads classified on the node, and the red spheres represent un-annotated V-, D- and J-gene (Figure 2A). Similarly, the length of each bar on IGL gene represents the number of reads classified on the node, and the un-annotated V- and J-gene were represented on the far right (Figure 2B).

Antibody-gene synthesis and expression

Synthesized VDJ sequences were selected from output reads of NGS and cloned into mammalian antibody expression vectors (TOYOBO). I picked four clones of antibody sequences for each experimental group. CHO cells were transfected with the gene constructs and screened using puromycin (10 mg/mL). Antibodies secreted into culture medium were tested using ELISA for binding to NP and CGG.

ELISA

To test the antigen-antibody reactivity of the expressed proteins, Flat-bottomed 96-well plates (Immuno-MaxiSorp; Nunc 442404) were coated with 5μg/mL of NP-CGG or CGG and incubated at 4℃ overnight, followed by blocking with 1% BSA in PBS/0.05% Tween 20 (Sigma, P-1379). Supernatants were harvested after 24 hours for transient transfection and approximately 20 days for stable transfection. Supernatants incubation and HRP-anti-mouse antibodies incubation are all at 37℃ for one hour. Hydrogen peroxide in citrate buffer and O-phenylenediamine (Invitrogen, 002003) were used as the chromogen and optical density was measured at 490nm.

Results

I used NGS of Roche 454 system initially to analyze the overall amplified sequence of antibody genes for individual mice. Total RNA from the spleen was reverse-transcribed and the fragments containing VDJ/VJ and partial CH1 were amplified by using 5'-RACE universal adapter and 3'-CH1 primers. In order to visualize the NGS data of holistic aspects of B cell repertoires for these individual mice, I used a simple and confirmative method to decipher these repertoires that was developed by my group (Kono, Sun et al. 2017).

Raw reads obtained from NGS were translated to amino acid in six reading-frames and checked if it has a defined discernment sequence of each immunoglobulin class. The sequences with productive VDJ junction were collected. I used the program designed by my group to visualize the overall perspective of the antibody repertoire. The reads of IgH repertoires were arrayed on the three-dimensional mesh (3D-VDJ-plots) in which x-axis represents 110 x IGHV genes, y-axis represents 12 x IGHD genes and 4 x IGHJ genes, and IgL repertoires were arrayed on the two-dimensional diagram (2D-VJ-plots) in which x-axis represents 110 x IGLVκ and 4 x IGLVλ genes, y-axis represents 4 x IGLJκ and 4 x IGLJλ genes (Figure 2). The order of the genes in the plot mesh is the same order as theire locations on the chromosomes. The volume of each sphere on IGH gene represents the

number of reads classified on the node, and the red spheres represent un-annotated V-, D- and J-gene (Figure 2A). Similarly, the length of each bar on IGL gene represents the number of reads classified on the node, and the un-annotated V- and J-gene were represented on the far right (Figure 2B).

To obtain an overview on the dynamics of entire antibody repertoires during the antigen response, I analyzed immunoglobulin transcripts from entire spleens of five individual mice for each group of antigen immunization. Antibody repertories of naive, NP-hapten or CGG-carrier immunized mice were analyzed by NGS. From each run, approximately 10^4 reads containing productive VDJ junctions were collected by using Roche 454 system. The VDJ-rearrangement profile in individual mice was displayed on 3D-VDJ-plots. Antibody repertoires of naive and immunized mice were analyzed by comparison of the IgG1 sequences from five each individual mouse. As I expected, IgG1 repertoires of individual naive mice were not correlated. On the other hand, for NP-CGG-immunized and CGG-immunized group, commonly used antigen-specific IgG1 repertoires were observed in each group. The major IGHVs commonly observed in NP-CGG-immunized group was IGHV1-72, and in CGG-immunized group was IGHV9-3. IGHV1-72, also known as $V_H186.2$, is a widely recognized anti-NP antibody in C57BL/6 mice. This result showed the viability of this prediction protocol. To confirm the antigen specificity of these

repertories, I synthesized the antibody genes for a randomly selected VDJ sequence from the IGHV1-72/ IGHD1-1/IGHJ2 and IGHV9-3/IGHD3-1/IGHJ2 repertories, respectively, and cloned into an antibody-expression vector of mammalian express system. As for NP-CGG antibody gene, I synthesized the read from IGHV1-72/ IGHD1-1/IGHJ2 pairing with already-known NP-specific Vλ1-LC. On the other hand, I synthesized the read from IGHV9-3/IGHD3-1/IGHJ2 pairing with the same Vλ1-LC for CGG antibody gene. These antibodies were transfected to CHO cells and the secreted antibodies were tested by using ELISA for binding to NP and CGG. The ELISA results showed the high reactivity of IGHV1-72 against NP-CGG, whereas a lower level but significant response was showed of IGHV9-3 against CGG (Figure 3).

One NGS run was used for mice of the same immunization status. From each run, approximately 10^4 reads containing productive VDJ junctions were collected by using Roche 454 system. Meanwhile, I tried another system, MiSeq system, and approximately 10^6 reads containing productive VDJ junctions were collected from each run (Figure 4). 100-fold increase was confirmed by using MiSeq system.

Discussion

I performed NGS analysis on antibody RNAs amplified using the 5'-RACE method. With this method, the whole views of B cell repertoires in individual mice could able to be visualized for each antibody subclass. The global expression patterns of antibody repertoires of individual naive mice revealed that the no common VDJ profile of IgG1 was appeared. On the contrary, antigen immunized groups showed strong correlation of VDJ profiles of IgG1 in both NP-CGG-immunized and CGG- immunized group. This implies that immunization increased a specific set of VDJ profiles of mice with the same genetic background. The common usage of IGHV1-72 for NP that showed the identical to well-known anti-NP antibody, $V_H186.2$, indicated that this method to detect the antigen-specific repertoire is successful. With this simple prediction protocol, my group described CGG-specific antibody, IGHV9-3, for the first time. ELSA test of expressed antibody protein that encoded by selected genes showed the antigen specificities of the antibodies. Although IGHV9-3 antibody showed a significant response against CGG, the affinity was low compared to that of NP-binding of IGHV1-72 antibody. In the antibody expression system I employed, it is difficult in the nomination of specific-IgL for the NGS-predicted IgH because the NGS-method does not infer the intrinsic IgH-IgL pairs. Thus, it must be established the new method determining the LC pairing to the

18

corresponding HC, or a "universal LC" that can be associates with diverse HCs species without losing its antigen-binding properties.

My attempt of using another NGS system, MiSeq system, showed the higher throughput for one run, approximately 100-fold increase, compared to Roche 454 system. I henceforth used the MiSeq system to decipher antibody repertoires.

Chapter 2

Characterization of Antibody Repertoire Developed in the Absence of

Pre-BCR Formation

Introduction

The pre-BCR marks an important checkpoint during early B cell development, as only cells that have successfully recombined the μHC gene locus are allowed to progress onwards (Karasuyama, Kudo et al. 1990, Tsubata and Reth 1990). At this stage of development, newly produced μHC assembles with the invariant SLC to form a pre-BCR, where association with the SLC serves as a quality check of μHCs (Almqvist and Martensson 2012). In contrast to conventional LCs that consisted from a single polypeptide, the pre-BCR is consisted from two polypeptides, Vpre-B and λ5. Vpre-B shows homology to IgV regions and λ5 to the constant region of λLCs, and each peptides carries a unique non-Ig tails (Melchers, Karasuyama et al. 1993, Melchers 2005). Different from conventional BCR that need external ligands, pre-BCR is able to be activated autonomously. The non-Ig portion of λ5 is crucial for autonomous aggregation, internalization and signaling of the pre-BCR. Particularly, the functional domain of λ5 is attributable to its conserved charged Arg residues that contacting neighboring μHCs (Ohnishi and Melchers 2003). The structural features of λ5 unique tail are well studied. However, little is known about the role of the unique region of Vpre-B (Dimitrov, Planchais et al. 2013) .

In this study, I use λ5 knockout ($\lambda5^{-/-}$) mice as an experimental model. This animal

model has severed defected of B cell development in bone marrow. And the phenotype is similar to those lacking Vpre-B or entire SLC mice. The interesting characteristic of these SLC-deficient mice is the generation of a significant number of mature B cells, leaky B cell, without pre-BCR formation. Moreover, several reports revealed that SLC-deficient mice showed a similarity to aged WT mice of autoreactivity owning to diminished levels of $\lambda 5$ and Vpre-B (Ratliff, Alter et al. 2013, Ratliff, Alter et al. 2015). Because the young $\lambda 5^{-/-}$ mice, as well as aged mice are resistant to cytokine-induced apoptosis and shows increased apoptosis. It is affecting the readout of the antibody repertoire and promoting autoreactivity within the naïve antibody repertoires (Ratliff, Alter et al. 2015). However, even several studies showed the autoreactivity of $\lambda 5^{-/-}$ mice (Shimizu, Mundt et al. 2002, Keenan, De Riva et al. 2008, Kohler, Hug et al. 2008), I have not observed any developmental defects or short-living for over 24 months of ages. I suppose that there must be several mechanisms operated in both primary and secondary lymphoid organs in $\lambda 5^{-/-}$ mice to avoid autoreactivity.

In order to explore the function of SLC, I used NGS to analyze the sequences of antibody transcripts for individual WT or $\lambda 5^{-/-}$ littermates. Initially, I raised two possible pathways for the generation of leaky B cells: 1) Particular IgL may rearranged prior to IgH, and differentiate into immature B cells (Kitamura, Kudo et al. 1992); 2) Generating

from B1 cells that derived from the neonatal liver (Doran, Benzie et al. 1974, Owen, Raff et al. 1976) or the peritoneal cavity (Kitamura, Kudo et al. 1992). The VDJ-usage frequency profiles of spleen B cell repertoires showed the different pattern of sequence convergence between WT and $\lambda 5^{-/-}$ mice. However, there is no special VJ-usages in $\lambda 5^{-/-}$ mice of spleen B cell that negated my first pathway. My pathway 2 is also negated by the analysis of sorted spleen B cell of B1 population.

To assess the underlying causes of the different pattern of VDJ-usages but not VJ-usages, I examined the amino acid distribution. CDR-H3 loops of bone marrow B cells but not spleen B cells showed characteristics signature with high portion of Arg in top-ranking CDR-H3 sequences of $\lambda 5^{-/-}$ mice. This interesting phenomenon suggest a specific role for CDR-H3 sequences in the formation of antibody repertoires.

Collectively, my findings defined a characteristic of $\lambda 5^{-/-}$ mice with particular pattern of spleen B cell repertoires, and high portion of Arg at the center of bone marrow CDR-H3 loop. Taken together, my approach provides the unique aspect of pre-BCR function in the antibody repertoire formation.

Materials and Methods

Mice and ethics statements

This was performed as described in Chapter 1.

RNA preparation and cDNA synthesis

This was performed as described in Chapter 1.

PCR amplification in MiSeq system

This was performed as described in Chapter 1.

Antibodies and reagents

The following antibodies were purchased from BioLegend: Brilliant Violet 510-Streptavidin (catalog number, 405233; working dilution, 1:100), PE/Cy5-anti-mouse TER-119 (116210; 1:100), APC-anti-mouse CD21 (123411; 1:100), Brilliant Violet 605-anti-mouse IgM (406523; 1:100), FITC anti-mouse CD5 (100606; 1:100), Biotin anti-mouse CD3ε (100304; 1:100), Biotin anti-mouse Ly-6G/Ly-6C (108404; 1:100), Biotin anti-mouse TER-119 (116204; 1:100). The following antibodies and reagents were purchased from BD Biosciences: APC anti-mouse CD45R/B220 (553092; 1:100), FITC

anti-mouse CD3ε (553061; 1:100). PE-anti-mouse CD23 (01235B; 1:100) was purchased from BD Pharmingen and Pacific Blue-anti-mouse/human CD45R/B220 (57-0452-82; 1:100) was purchased from eBioscience.

Flow cytometry

For phenotypic analysis of peripheral blood B cells, blood was collected from 4- to 30-week-old animals. B cells were treated with 2.4G2 (20 μg/mL) for 30 min on ice and then stained with PE/Cy5-anti-Ter-119, APC-anti-B220, FITC-anti-CD3ε in staining buffer (Hank's Balanced Salt Solution (HBSS) containing 1% bovine serum albumin and 0.05% sodium azide) for 60 min on ice (working dilutions are provided in the antibodies and reagents section).

For phenotypic analysis of spleen B cells, cell suspensions were prepared from spleens isolated from 8-week-old littermates. Spleen cells were treated with 2.4G2 for 30 min on ice and then stained with lineage drain antibodies (Biotin-anti-CD3ε, Biotin-anti-Gr-1, Biotin-anti-Ter-119) and Pacific Blue-anti-CD45R/B220, PE-anti-CD23, Brilliant Violet 605-anti-IgM, FITC anti-CD5, APC-anti-CD21 and Brilliant Violet 510-Streptavidin. Stained cells were analyzed on FACSAria III fluorescence flow cytometer (BD Biosciences).

Amino Acid Sequence Analysis on CDR-H3 region

The amino acid sequences of CDR-H3 region (IMGT-definition) were obtained for the output of IgBLAST. For each CDR-H3 sequence, I calculated the following two amino acid descriptors. 1) Kidera factor: The descriptors were originally described by applying multivariate analysis to 188 physical properties of the twenty amino acids by Kidera et al. (Kidera, 1985). The factors were calculated using the ''Kidera'' function of R. 2) AaWtLpR index was defined as the index that express relative position of specific amino acid in the CDR-H3 loops. For example, the relative position index of Asp in the CDR-H3 loop was calculated as follows.

$$\text{WtLpR}_{\text{Asp}} = \sum_{\text{Asp}} \left(1 - \left| \frac{\left(i - \frac{L}{2} \right)}{\left(\frac{L}{2} \right)} \right| \right) \qquad (1 \leqq i \leqq L)$$

Where L is the length in amino acid number of CDR-H3, and i is the position of specific amino acid, aspartic acid (Asp), in the CDR-H3. I calculated WtLpR index for twenty amino acids for each. The primary component analysis were performed using the "princomp" function of R-resource.

Multivariate analysis

Cluster analysis of VDJ and VJ profiles of individual mice was performed using Nk array data and ''hclust'' function in R ("ward" method with "canberra" distance) as

described in Kono et al. Pearson's correlation coefficients for IGHV usage were

calculated between individual mice, using the array of IGHV usage frequency in each

mouse.

Visualization of the V(D)J repertoires

This was performed as described in Chapter 1.

Results

B cells generated in λ5⁻/⁻ mice

In $\lambda5^{-/-}$ mice, significant numbers of peripheral B cells were observed, even though B cell development in the bone marrow is severely impaired in the absence of pre-BCR (Figure 5A). Intriguingly, these B cells somehow circumvented the pre-BCR checkpoint and, hence, their development is pre-BCR-independent. These leaky B cells comprise 2.7% of blood lymphocytes, in ~1/20 of 4-week-old WT mice (52.2%), and reach approximately 10%, in ~1/5 of WT mice, by 25-30 weeks of age (Figure 5B).

Initially, I considered two possible pathways for the generation of leaky B cells: 1) During the differentiation of B2 cells, a few precursor B cells may display a particular IgL, rearranged in the absence of pre-BCR, and differentiate into immature B cells, without an extensive clonal expansion (Figure 6 (arrow 1)); 2) leaky B cells are generated from B1 cells derived from the neonatal liver or the peritoneal cavity. Pre-BCR has little influence on B1 cell differentiation, due to their self-renewing properties (Kitamura, Kudo et al. 1992) (Figure 6 (arrow 2)). To address these potential pathways, I used NGS to analyze the sequences of antibody transcripts for individual WT or $\lambda5^{-/-}$ littermates. More importantly, elucidating the antibody repertoires in these leaky B cells would reveal the intrinsic role(s) of the pre-BCR in the formation of the antibody system.

Deep sequencing of IgH usage repertoire of λ5$^{-/-}$ mice and WT littermates

Spleens from naive 9-week-old naïve WT and λ5$^{-/-}$ mice were used for analyzing the B

cell repertoire of IgM, IgG1 and IgG2c (Figure 7) antibody subclasses. The VDJ-usage

frequency profiles of naïve IgM were highly correlated within each group. The VDJ

repertoire of λ5$^{-/-}$ mice showed the preferential usage of certain IGH-V genes, such as

IGVH1-15, and 6-3 (Figure 8 upper panel), whereas WT mice commonly employed

IGVH11-2, 4-1 and 7-3 (Figure 8 middle panel). Interestingly, IGVH1-15 was also highly

expanded in IgG1 repertoire in λ5$^{-/-}$ mice (Figure 8 bottom panel) whereas no common

VDJ repertoires were shown for IgG1 in WT mice and IgG2c for both groups.

Furthermore, cluster analysis of the class-switched IGH gene usage showed partial

similarities, whereas the usage patterns for IgMs clearly differed between WT and λ5$^{-/-}$

littermates (Figure 9). Moreover, the VJ-usage profiles for Igκ and Igλ and the sequence

similarities for the Igκ repertoires, examined by clustering, clearly differed between WT

and λ5$^{-/-}$ littermates (Figure 10).

IgH and IgL repertoire patterns in peripheral B cell subpopulations in WT and λ5$^{-/-}$

mice

To examine repertoire patterns in B cell subpopulations, especially B1 cells, spleen cells were sorted into follicular (FO: Lin⁻B220⁺CD23^{high}) B cells, B1 (Lin⁻B220⁺CD23^{low}IgM^{high}CD5⁺) cells, marginal zone (MZ: Lin⁻B220⁺CD23^{low}IgM^{high}CD5⁻CD21⁺) B cells and transitional-2 (T2: Lin⁻B220⁺CD23^{low}IgM^{high}CD5⁻CD21⁻) B cells (Figure 11A). The FO and the T2 cell counts were 3.4-fold and 11.2-fold higher, respectively, in the WT than those in λ5$^{-/-}$ mice, whereas no differences were observed for the B1 and MZ cell counts (Figure 11B). The IgH and IgL repertoires of these sorted B cell subpopulations were analyzed by NGS.

The FO, B1, MZ, and T2 B cell IgM VDJ repertoires (Figure 12), and the similarities between WT and λ5$^{-/-}$ mice were assessed in each B cell compartment and analyzed by clustering (Figure 13A). I detected two separate clusters, B1/T2 and MZ/FO, with similar WT and λ5$^{-/-}$ repertoires within each cluster, suggesting that λ5$^{-/-}$ FO cells are not derived from B1 cells. Similarly, the IgL(κ/λ) VJ repertoires were compared for the sorted cell populations (Figure 14). The complexity of the λ5$^{-/-}$ IgL repertoires is comparable to that in WT mice, suggesting that leaky B cells in λ5$^{-/-}$ mice are not derived from precursor B cells in which the VJ-rearrangement occurred in the absence of pre-BCR. Cluster analysis also showed that the VJ repertoires of WT and λ5$^{-/-}$ mice were similar for each B cell compartment (Figure 13B). In addition, I investigated two well-known B1 genes Igκ4 and

Igκ9 (Hardy, Wei et al. 2004) to check the VJ distribution and no obvious deficiency were found in λ5$^{-/-}$ mice albeit with a reduced expression (Figure 15).

Different IgM repertoires are formed in the bone marrow of WT and λ5$^{-/-}$ mice

Because my previous hypotheses regarding leaky B cell generation were refuted, I examined the bone marrow B cell repertoires for differences between WT and λ5$^{-/-}$ mice. The IgM repertoires of four WT and four λ5$^{-/-}$ littermates were analyzed (Figure 14 and Figure 16). In WT mice, the VDJ combinations were relatively homogeneous, except that IGHV11-2 was preferentially used together with IGHJ1 and was commonly expanded in all four WT littermates. In λ5$^{-/-}$ mice, VDJ combinations were relatively sporadic and the IGHV11-2 expansion was not observed in any of the littermates.

CDR-H3 sequences were deduced from IgBLAST outputs and compared between WT and λ5$^{-/-}$ mice. When CDR-H3 sequences were sorted by their abundance, the usage frequencies of top-ranking CDR-H3s were significantly higher in λ5$^{-/-}$ than in WT mice Figure 17 A and B), suggesting the clonal expansion of restricted precursor B cell clones containing top-ranking CDR-H3 sequences.

To test whether the properties of the CDR-H3 amino acid sequences were different between WT and λ5$^{-/-}$ mice, I calculated physicochemical amino acid descriptors related

to the 3D-protein structure (Kidera, Konishi et al. 1985, Epstein, Barenco et al. 2014), using Kidera factors, for each CDR-H3 sequence. Moreover, I examined the differences between WT and $\lambda5^{-/-}$ mice using PCA. The physicochemical properties of CDR-H3s considerably differed between WT and $\lambda5^{-/-}$ mice (Figure 18), with the most dominant descriptor being "extended structure preference" in PC1 (Figure 19). I next performed a PCA analysis of same CDR-H3 sequences (Figure 18B), using factors expressing the relative position of each amino acid in the CDR-H3 loop (AaWtLpR, see Materials and Methods). Interestingly, the major descriptor in PC2 was the relative position of Arg(s) in the CDR-H3 loop (Figure 20). Thus, the top-ranking CDR-H3 sequences in $\lambda5^{-/-}$ mice preferentially contain Arg(s) in the middle of the CDR-H3 loop, compared to those in WT (Figure 17A, colored sequences). When bone marrow cells were sorted into pro/pre-B, immature B, and circulating B cell subsets (Figure 21), the Arg(s) in-the-middle-of-loop feature was not observed in pro/pre-B cells (Hardy's Fr. D, Fr. C and Fr. C′) (Hardy, Carmack et al. 1991) but was evident in immature B (Fr. E) and recirculating B cells (Fr. F) (Figure 22). Thus, VDJ-recombination normally occurs in pro/pre-B cells in $\lambda5^{-/-}$ mice, while the μHC containing Arg(s) in the middle of the CDR-H3 loop was positively selected and retained in immature B cells. Interestingly, the dissociation of CDR-H3 profiles observed in bone marrow B cells was not observed between WT and $\lambda5^{-/-}$ spleen

B cells (Figure 18C), suggesting that the distorted CDR-H3 repertoires were rectified during the peripheral transition. Moreover, based on bone marrow B cell repertoires, I propose a model for the leaky B cell generation pathway. The certain sequence convergence and center amino acid of Arg indicated an important role of Arg in $\lambda 5^{-/-}$ mice. Correlation with the signaling pathway proposed in pre-B cells (Ohnishi and Melchers 2003), the Arg(s) in bone marrow B cell CDR-H3 in $\lambda 5^{-/-}$ mice might taking the place of the Arg(s) in $\lambda 5$ protein (Figure 23). The Arg(s) in CDR-H3-loop in $\lambda 5^{-/-}$ mice is probably functional as in $\lambda 5$ protein which contained an array of evolutionary conserved Arg to induce proliferation and critical for B cell differentiation.

Discussion

To elucidate the role of pre-BCR in the formation of the antibody repertoire, I analyzed the full complement of BCR repertoires from spleens and bone marrows of WT and $\lambda 5^{-/-}$ mice using NGS. My initial two hypothetical models for the pre-BCR-independent leaky B cell generation were refuted: leaky B cells are derived neither from the B1 cell compartment nor from the synthesis of a particular LC that compensates for SLC. In $\lambda 5^{-/-}$ bone marrows, substantial levels of productive IgM class VDJ-rearrangements were observed.

Intriguingly, particular CDR-H3 sequences were preferentially enriched in IgM^+ B cells in $\lambda 5^{-/-}$ bone marrows. Since it is unlikely for different clones to give rise to the same CDR-H3 sequence, the enrichment observed in $\lambda 5^{-/-}$ bone marrows strongly suggests the clonal expansion of these precursor B cells in the absence of pre-BCR. When analyzing CDR-H3 properties using Kidera factors, differences in $\lambda 5^{-/-}$ CDR-H3s became obvious. This dissociation was also evident using simple amino acid descriptors calculated from the relative position of the twenty amino acids. Here, the most significant parameter was the relative position of Arg(s) in the CDR-H3 loop. In fact, about half of the top-ranking $\lambda 5^{-/-}$ CDR-H3 sequences contain Arg(s) in the middle of this loop, as opposed to WT sequences. When fractionating bone marrow B cells using Hardy's Fr. D (plus C and C′),

Fr. E, and Fr. F, the dissociation of CDR-H3 sequences was not observed in Fr. D (plus C and C′), suggesting that the VDJ-rearrangement is not biased in the absence of λ5. However, the dissociation become obvious in the Fr. E and Fr. F populations, suggesting that only a part of the non-biased VDJ-rearrangements in Fr. D, those containing the dissociated feature of CDR-H3s, passed the pre-BCR checkpoint.

These results strongly suggest that the Arg(s) in the CDR-H3 loop compensate for the absence of SLC. Arg in the non-Ig portion of λ5 were required for constitutive internalization and signaling of the pre-BCR (Ohnishi and Melchers 2003). Thus, Arg(s) in the middle of the CDR-H3 loop may play a similar role and compensate for the absence of SLC, giving rise to leaky B cells. Unlike the other positively charged amino acids, Arg solubilizes protein aggregates (Hirano, Kameda et al. 2013). It is therefore possible that the strong positive charge and the potent solubilization ability of Arg underlie the specific interaction mode of biomolecules with the CDR-H3 loop.

The pairing of the nascent IgH with the SLC configures an important checkpoint that controls and selects for IgH species (ten Boekel, Melchers et al. 1997, Rolink, Brocker et al. 1999, Hardy, Wei et al. 2004, Kawano, Yoshikawa et al. 2005, Grimsholm, Ren et al. 2015). CDR-H3 differences may affect the pairing ability of SLC. Therefore, Arg(s) in the CDR-H3 loop may impair SLC pairing and induce apoptosis in WT, but not in λ5$^{-/-}$ B

cells. Thus, Arg-containing CDR-H3s would persist in the λ5$^{-/-}$ repertoire. However, this explanation does not account for the clonal expansion of Arg-containing CDR-H3s.

Accumulating evidence suggests that the pre-BCR checkpoint prevents autoreactivity in nascent µHCs, acting as a surrogate autoreactive receptor (Keenan, De Riva et al. 2008, Almqvist and Martensson 2012, Melchers 2015). In addition, the weak autoreactivity of pre-BCR may represent a driving force for the positive selection of B cells in the bone marrow (Herzog and Jumaa 2012, Melchers 2015). My present data strongly support this viewpoint. When assessing the whole repertoire of bone marrow µHC in λ5$^{-/-}$ mice, only CDR-H3s with specific feature(s) passed the pre-BCR checkpoint, and autoreactive CDR-H3s (containing Arg(s)) were expanded in the absence of λ5. These autoreactive µHC repertoires were soon negatively selected in the process of peripheral transfer, at the third and fourth checkpoint in B cell development (Melchers 2015). However, these repertoires remain skewed, while peripheral VDJ repertoires are distorted in λ5$^{-/-}$ mice. Nevertheless, the antibody response against NP-CGG was comparable in WT and λ5$^{-/-}$ mice, except for the ratio of the high affinity IgM antibody. These results suggest the presence of robust mechanism(s) for the correction of skewed antibody repertoires. I am currently analyzing the mechanism underlying the selection of B cell clones with dissociated CDR-H3 sequences.

Chapter 3

Long-term Observation of Immune Response against NP-CGG in

WT and $\lambda 5^{-/-}$ Mice

Introduction

B cell development and differentiation proceeds with multiple checkpoints. The first checkpoint depends on SLC molecules that probe IgH fitness to pair with LCs. The second checkpoint is based on pre-BCR formation. These two checkpoints impaired in $\lambda 5^{-/-}$ mice. However, there are still significant numbers of leaky B cells generated in $\lambda 5^{-/-}$ mice. Several reports suggested that the pool of naïve B cells in $SLC^{-/-}$ mice is skewed for autoreactivity (Keenan, De Riva et al. 2008, Grimsholm, Ren et al. 2015). Since I have not observed any particular pathology for over 24 months in $\lambda 5^{-/-}$ mice, multiple checkpoints would be worked to prevent autoimmune diseases in the mouse immune system. Newly formed autoreactive B lymphocytes can be eliminated in the bone marrow through clonal deletion at the third checkpoint. Based on the analysis of bone marrow antibody repertoires, $\lambda 5^{-/-}$ mice showed a specific feature of distorted antibody repertoire. At the fourth checkpoint, immature B cells with potential autoreactivity undergo receptor editing or they are eliminated before they mature. The newly formed B cells in $\lambda 5^{-/-}$ mice proceed their differentiation through these checkpoints and develop into mature B cells with skewed spleen antibody repertoires. Through these processes, finally generated mature B cells recognize foreign antigens. The important point of antigen-antibody reaction is the formation of FO and GC, in which B cells undergo affinity maturation,

class-switch recombination to yield high-affinity plasma cell (PC) and memory B cells (MBC) (Manz, Thiel et al. 1997). In $\lambda 5^{-/-}$ mice, it is established that the immune response against T cell-dependent antigen NP-CGG was attenuated for lgG3 and IgG2b antibodies compared to IgG1 antibodies during early stage (Kitamura, Kudo et al. 1992). Because MBC and long-lived PC are responsible for immunological "memory", I examined the immune response against NP-CGG over long periods of time to compare the antibody producing ability. In addition, I examined the autoantibodies against single-stranded DNA (ssDNA) and double-stranded DNA (dsDNA), because Arg in the CDR-H3 loop is a characteristic feature of many autoreactive antibodies.

Materials and Methods

Mice and ethics statements

This was performed as described in Chapter 1.

Immunizations

WT and $\lambda 5^{-/-}$ littermates were immunized intraperitoneally with 50 µg of NP-CGG precipitated with 100µL of Imject Alum adjuvant (Thermo Scientific, 77161). For the secondary antibody response experiments, littermates were immunized intravenous with 2.5 µg of NP-CGG 57 weeks later.

ELISA

For reactivity with model antigens, Flat-bottomed 96-well plates were coated with 1 µg/mL of NP-BSA and incubated at 4℃ overnight, followed by blocking with 1% BSA in PBS/0.05% Tween 20. Sera were used 1:100 dilutions in PBS/0.05% Tween 20 and serially diluted for antibody titers test. NP-specific monoclonal antibodies (established in-house) were used as standards to calculate the relative antibody titers and affinities. For autoantibodies detecting, 5 µg/mL of ssDNA or dsDNA were coated at 4℃ overnight, followed by blocking with 1% BSA in PBS/0.05% Tween 20. Sera were used 1:20

dilutions in PBS/0.05% Tween 20 and serially diluted for antibody titers test. MRL mice sera were used 1:50 dilutions as standards to calculate the relative antibody titers and affinities. Sera incubation and HRP-anti-mouse antibodies incubation are performed at 37℃ for one hour. Hydrogen peroxide in citrate buffer and O-phenylenediamine were used as the chromogen and optical density was measured at 490nm.

Statistical analysis

Microsoft Excel was used for statistical analysis. The error bars on the figures represent the standard deviation from the mean. Significances of differences between experimental values were tested using Student's t-test.

Results

Immune responses against T-dependent antigen worked almost normally in $\lambda 5^{-/-}$ mice.

In order to investigate the immune response without pre-BCR checkpoint during early B cell development, WT and $\lambda 5^{-/-}$ mice were immunized with model antigen NP-CGG and antigen-specific serum antibody titers were measured over a long period of time (Figure 24). There were small but significant differences in high affinity IgM response during the first 1-4 weeks post-immunization, indicating that the initial immune response of $\lambda 5^{-/-}$ mice is affected by the $\lambda 5$ deficiency. Since no significant differences were detected in the later stages of immune response, I examined secondary antibody responses against NP-CGG. Littermates were boost immunized with an intravenous injection of NP-CGG 57 weeks later after the primary immunization. NP-specific serum antibody titers at Day 10 after the boost were compared with those before the boost. No significant differences were detected between WT and $\lambda 5^{-/-}$ mice (Figure 25). These results indicated the secondary antibody response is unaffected by $\lambda 5$ deficiency.

Antibody responses against ssDNA and dsDNA did not show statistically significant difference between WT and $\lambda 5^{-/-}$ mice

The autoreactivity is always conferred by a high proportion of basic amino acids in the CDR-H3. My bone marrow antibody repertorie analysis also showed the preference of containing Arg(s) in the middle of the CDR-H3 loop in $\lambda 5^{-/-}$ mice. Moreover, long-term observation of immune response against NP-CGG also showed the higher response lever against NP without immunization (Figure 24A). Therefore, I checked autoantibodies against ssDNA and dsDNA for naive 10-week-old littermates (Figure 26). Antibodies titers in $\lambda 5^{-/-}$ mice were raised slightly higher than these in WT mice, in cases of IgM, IgG2b and whole IgG against ssDNA and dsDNA. However, the differences were not statistically significant. In case of IgG3 against ssDNA and dsDNA, there was no difference between WT and $\lambda 5^{-/-}$ mice.

Discussion

My results showed that $\lambda 5^{-/-}$ mice are capable of producing antigen-specific antibodies without the experience of checkpoints exerted by pre-BCR formation. However, the high affinity antibody response against NP-CGG in $\lambda 5^{-/-}$ mice showed weak impairment during the early stage of primary response. It was probably due to the lack of pre-BCR induced cloned expansion of B cells in $\lambda 5^{-/-}$ mice. On the other hand, the long-term observation of primary responses and boost immunization exhibited almost equal NP-specific antibody titers between WT and $\lambda 5^{-/-}$ littermates. It indicated that the $\lambda 5^{-/-}$ mice were also able to induce almost normal immune responses, including memory B cell formation.

Nevertheless, the higher response lever of "NP-specific" IgM antibody was detected in $\lambda 5^{-/-}$ mice before immunization of NP-CGG antigen. Here, I investigated the serum autoantibodies against ssDNA and dsDNA. The binding antibodies titers were raised slightly in $\lambda 5^{-/-}$ mice than in WT for IgM, IgG and IgG2b. These differences did not achieve statistical significance. Without the SLC formation, the first and second checkpoints were excluded, giving rise Arg(s) in the CDR-H3 loops. These Arg(s) would likely cause poly-reactive affinity to broad antigens including NP-CGG, ssDNA and dsDNA. However, the result of antibody response against ssDNA and dsDNA did not show the autoreactivity in $\lambda 5^{-/-}$ mice.

My results of bone marrow antibody analysis showed that only CDR-H3s with specific feature(s) passed the pre-BCR checkpoint, and autoreactive CDR-H3s (containing Arg(s)) were expanded in the absence of λ5.

In conclusion, my present data strongly support the viewpoint that weak autoreactivity of pre-BCR may represent a driving force for the positive selection of B cells in the bone marrow (Herzog and Jumaa 2012, Melchers 2015). In $λ5^{-/-}$ mice, autoreactive μHC repertoires were soon negatively selected in the process of peripheral transfer at the third and fourth checkpoint. However, these repertoires remain skewed, while peripheral VDJ repertoires are distorted in $λ5^{-/-}$ mice. Nevertheless, the antibody response against NP-CGG was comparable in WT and $λ5^{-/-}$ mice, except for the ratio of the high affinity IgM antibody. These results suggest the presence of robust mechanism(s) for the correction of skewed antibody repertoires. I am currently analyzing the mechanism underlying the selection of B cell clones with dissociated CDR-H3 sequences.

General Discussion

NGS is a powerful tool for describing and analyzing the overall B-cell repertoires and their dynamic changes in individual immune systems. By applying the MiSeq system to decipher antibody repertoires system, I obtained high resolution with the reads of approximately 10^6 for each run that was 100-fold increase compared to Roche 454 system.

Here, I used NGS to analyze the pre-BCR function by outlining the BCR repertoires from spleen and bone marrow of WT and $\lambda 5^{-/-}$ mice to elucidate how B cells develop without the pre-BCR formation.

Spleen B cell repertoires showed different profiles between WT and $\lambda 5^{-/-}$ mice. IGHV11 rearrangements which combine with $IGLV_k 9$ have found in natural autoantibodies expressing CD5 and together with IGHV12 which combined with $IGLV_k 4$ are termed B1 cell (Hardy, Wei et al. 2004). I confirmed IGHV11 convergence but not IGHV12 in splenic B cell repertoires and serum B cell repertories. $IGLV_k 9$ usage also showed no significant differences between WT and $\lambda 5^{-/-}$ mice. These results implied the IGHV11 in my data may reveal other characteristics of B cells. IGHV4-2 and IGHV6 genes are reported to be strongly associated with autoimmune reactivity in human (Deane, Baker et al. 1993, Raaphorst, Langlois van den Bergh et al. 1997) but not in mice, and highly restricted usage of IGHV14-2 gene is proved in Slp65-deficient pre-B cell leukemia in

mice (Ta, de Bruijn et al. 2012) . IGHV1-15 gene was well-converged in both IgM and

IgG1 B cells from $\lambda 5^{-/-}$ mice. This gene belongs to the very large VhJ558 family, which

contributes little to the fetal repertoire but represented much in splenic B cell repertoires

(Haines, Angeles et al. 2001, Schroeder 2006). Further investigation is required to reveal

the characteristics of IGHV1-15 about how class switching occurs without antigen

activation or is it associated with antoreactivity.

Structural investigations showed that the unique tails of the SLC playing an important

role in probing of μHC for their capacity to form qualified BCR (Kohler, Hug et al. 2008).

The unique tails extend over the antigen-binding site of HC and cover the CDR-H3 loop.

Meanwhile, the CDR-H3 encoded by the VDJ junction, is the most variable of the three

CDR-3s that plays a vital role in recognition of both antigen and autoantigen (Winkler,

Fehr et al. 1992, Radic and Weigert 1994, Xu and Davis 2000, Vale, Kapoor et al. 2013).

The differences between WT and $\lambda 5^{-/-}$ mice of spleen B cell repertories should also be

reflected in the amino acid distribution of CDR-H3-loop. However, there were no

significant differences between them. This seemingly paradoxical phenomenon most

likely indicates that multiple checkpoints must be exerting the effects on negative

selection to prevent the production of autoantibodies in $\lambda 5^{-/-}$ mice.

Flow cytometric analyses of spleen B cells revealed a dramatic decrease of T2 B cells

in $\lambda5^{-/-}$ mice. As T2 B cell is the immediate precursor of the mature B cell populations derived from bone marrow (Su, Guo et al. 2004), I investigated the bone marrow B cell repertoires with CDR-H3 properties using Kidera factors. The usage frequencies of top-ranking CDR-H3s were significantly higher in $\lambda5^{-/-}$ mice, and these top-ranking CDR-H3 sequences preferentially contain Arg(s) in the middle of CDR-H3 loop. A possible scenario for the events taking place in the bone marrow could be the elevated Arg(s) are used in place of non-Ig tail in $\lambda5$ to induce self-crosslinking. The leaky B cells generated in $\lambda5^{-/-}$ mice is partly dependent on Arg(s) in the CDR-H3 loops which in normal pathway is derived from $\lambda5$. Therefore, in the case of $\lambda5^{-/-}$ mice, the signaling to clonal expansion is probably coming from HC. In human, approximately 9 % of in-frame μHC transcripts are found expressed on the cell surface in the absence of SLC (Minegishi and Conley 2001). This phenomenon seems to be an analogy to my results observed in mice. About half of leaky B cells do not possess Arg(s) in the middle of the CDR-H3 loop, suggesting that other CDR-H3 features may play a similar role in generating leaky B cells.

Several reports showed that the weak autoreactivity of pre-BCR may represent a driving force for the positive selection of B cells in the bone marrow (Herzog and Jumaa 2012, Melchers 2015). However, these leaky B cells in $\lambda5^{-/-}$ mice will still enter the third

and fourth checkpoint in B cell development with the skewed repertoires. The data I presented in this study confirm this viewpoint of B cell development in that the Arg(s) in CDR-H3 drives the clonal expansion of precursor B cells and the population is negatively selected partly in the later stage(s) of B cell development.

In conclusion, I showed the distorted antibody repertoire development in the absence of pre-BCR formation, and the existence of the robust compensation mechanism(s) on the distorted antibody repertoire caused by the absence of pre-BCR, using the newly developed NGS method for the visualization of holistic feature of antibody repertoire.

Acknowledgments

References

Almqvist, N. and I. L. Martensson (2012). "The pre-B cell receptor; selecting for or against autoreactivity." Scand J Immunol **76**(3): 256-262.

Cumano, A. and K. Rajewsky (1985). "Structure of primary anti-(4-hydroxy-3-nitrophenyl)acetyl (NP) antibodies in normal and idiotypically suppressed C57BL/6 mice." Eur J Immunol **15**(5): 512-520.

Deane, M., B. W. Baker and J. D. Norton (1993). "Immunoglobulin VH4 gene usage in B lymphoid leukaemias." Br J Haematol **84**(2): 242-249.

Dimitrov, J. D., C. Planchais, L. T. Roumenina, T. L. Vassilev, S. V. Kaveri and S. Lacroix-Desmazes (2013). "Antibody polyreactivity in health and disease: statu variabilis." J Immunol **191**(3): 993-999.

Doran, T. A., R. J. Benzie, J. L. Harkins, V. M. Owen, C. J. Porter, D. W. Thompson and S. I. Liedgren (1974). "Amniotic fluid tests for fetal maturity." Am J Obstet Gynecol **119**(6): 829-837.

Epstein, M., M. Barenco, N. Klein, M. Hubank and R. E. Callard (2014). "Revealing individual signatures of human T cell CDR3 sequence repertoires with Kidera Factors." PLoS One **9**(1): e86986.

Furukawa, K., A. Akasako-Furukawa, H. Shirai, H. Nakamura and T. Azuma (1999). "Junctional amino acids determine the maturation pathway of an antibody." Immunity **11**(3): 329-338.

Georgiou, G., G. C. Ippolito, J. Beausang, C. E. Busse, H. Wardemann and S. R. Quake (2014). "The promise and challenge of high-throughput sequencing of the antibody repertoire." Nat Biotechnol **32**(2): 158-168.

Grimsholm, O., W. Ren, A. I. Bernardi, H. Chen, G. Park, A. Camponeschi, D. Chen, B. Bergmann, N. Hook, S. Andersson, A. Stromberg, I. Gjertsson, S. Cardell, U. Yrlid, A. De Riva and I. L. Martensson (2015). "Absence of surrogate light chain results in spontaneous autoreactive germinal centres expanding V(H)81X-expressing B cells." Nat Commun **6**: 7077.

Haines, B. B., C. V. Angeles, A. P. Parmelee, P. A. McLean and P. H. Brodeur (2001). "Germline diversity of the expressed BALB/c VhJ558 gene family." Mol Immunol **38**(1): 9-18.

Hardy, R. R., C. E. Carmack, S. A. Shinton, J. D. Kemp and K. Hayakawa (1991). "Resolution and characterization of pro-B and pre-pro-B cell stages in normal mouse bone marrow." J Exp Med **173**(5): 1213-1225.

Hardy, R. R., C. J. Wei and K. Hayakawa (2004). "Selection during development of VH11+ B cells: a model for natural autoantibody-producing CD5+ B cells." Immunol Rev **197**: 60-74.

Herzog, S. and H. Jumaa (2012). "Self-recognition and clonal selection: autoreactivity drives the generation of B cells." Curr Opin Immunol **24**(2): 166-172.

Hirano, A., T. Kameda, D. Shinozaki, T. Arakawa and K. Shiraki (2013). "Molecular dynamics simulation of the arginine-assisted solubilization of caffeic acid: intervention in the interaction." J Phys Chem B **117**(25): 7518-7527.

Karasuyama, H., A. Kudo and F. Melchers (1990). "The proteins encoded by the VpreB and lambda 5 pre-B cell-specific genes can associate with each other and with mu heavy chain." J Exp Med **172**(3): 969-972.

Karasuyama, H., A. Rolink, Y. Shinkai, F. Young, F. W. Alt and F. Melchers (1994). "The expression of Vpre-B/lambda 5 surrogate light chain in early bone marrow precursor B cells of normal and B cell-deficient mutant mice." Cell **77**(1): 133-143.

Kawano, Y., S. Yoshikawa, Y. Minegishi and H. Karasuyama (2005). "Selection of stereotyped VH81X-{micro}H chains via pre-B cell receptor early in ontogeny and their conservation in adults by marginal zone B cells." Int Immunol **17**(7): 857-867.

Keenan, R. A., A. De Riva, B. Corleis, L. Hepburn, S. Licence, T. H. Winkler and I. L. Martensson (2008). "Censoring of autoreactive B cell development by the pre-B cell receptor." Science **321**(5889): 696-699.

Kidera, A., Y. Konishi, M. Oka, T. Ooi and H. A. Scheraga (1985). "Statistical analysis of

the physical properties of the 20 naturally occurring amino acids." J. Prot. Chem. **4**(1): 23-55.

Kitamura, D., A. Kudo, S. Schaal, W. Muller, F. Melchers and K. Rajewsky (1992). "A critical role of lambda 5 protein in B cell development." Cell **69**(5): 823-831.

Kohler, F., E. Hug, C. Eschbach, S. Meixlsperger, E. Hobeika, J. Kofer, H. Wardemann and H. Jumaa (2008). "Autoreactive B cell receptors mimic autonomous pre-B cell receptor signaling and induce proliferation of early B cells." Immunity **29**(6): 912-921.

Kono, N., L. Sun, H. Toh, T. Shimizu, H. Xue, O. Numata, M. Ato, K. Ohnishi and S. Itamura (2017). "Deciphering antigen-responding antibody repertoires by using next-generation sequencing and confirming them through antibody-gene synthesis." Biochem Biophys Res Commun **487**(2): 300-306.

Manz, R. A., A. Thiel and A. Radbruch (1997). "Lifetime of plasma cells in the bone marrow." Nature **388**(6638): 133-134.

Melchers, F. (2005). "The pre-B-cell receptor: selector of fitting immunoglobulin heavy chains for the B-cell repertoire." Nat Rev Immunol **5**(7): 578-584.

Melchers, F. (2015). "Checkpoints that control B cell development." J Clin Invest **125**(6): 2203-2210.

Melchers, F., H. Karasuyama, D. Haasner, S. Bauer, A. Kudo, N. Sakaguchi, B. Jameson and A. Rolink (1993). "The surrogate light chain in B-cell development." Immunol Today **14**(2): 60-68.

Minegishi, Y. and M. E. Conley (2001). "Negative selection at the pre-BCR checkpoint elicited by human mu heavy chains with unusual CDR3 regions." Immunity **14**(5): 631-641.

Ohnishi, K. and F. Melchers (2003). "The nonimmunoglobulin portion of lambda5 mediates cell-autonomous pre-B cell receptor signaling." Nat Immunol **4**(9): 849-856.

Owen, J. J., M. C. Raff and M. D. Cooper (1976). "Studies on the generation of B

lymphocytes in the mouse embryo." Eur J Immunol **5**(7): 468-473.

Raaphorst, F. M., R. Langlois van den Bergh, J. L. Waaijer, J. M. Vossen and M. J. van Tol (1997). "Expression of the human immunoglobulin heavy chain VH6 gene element by fetal B lymphocytes." Scand J Immunol **46**(3): 292-297.

Radic, M. Z. and M. Weigert (1994). "Genetic and structural evidence for antigen selection of anti-DNA antibodies." Annu Rev Immunol **12**: 487-520.

Ratliff, M., S. Alter, D. Frasca, B. B. Blomberg and R. L. Riley (2013). "In senescence, age-associated B cells secrete TNFalpha and inhibit survival of B-cell precursors." Aging Cell **12**(2): 303-311.

Ratliff, M., S. Alter, K. McAvoy, D. Frasca, J. A. Wright, S. S. Zinkel, W. N. Khan, B. B. Blomberg and R. L. Riley (2015). "In aged mice, low surrogate light chain promotes pro-B-cell apoptotic resistance, compromises the PreBCR checkpoint, and favors generation of autoreactive, phosphorylcholine-specific B cells." Aging Cell **14**(3): 382-390.

Rolink, A. G., T. Brocker, H. Bluethmann, M. H. Kosco-Vilbois, J. Andersson and F. Melchers (1999). "Mutations affecting either generation or survival of cells influence the pool size of mature B cells." Immunity **10**(5): 619-628.

Schroeder, H. W., Jr. (2006). "Similarity and divergence in the development and expression of the mouse and human antibody repertoires." Dev Comp Immunol **30**(1-2): 119-135.

Shimizu, T., C. Mundt, S. Licence, F. Melchers and I. L. Martensson (2002). "VpreB1/VpreB2/lambda 5 triple-deficient mice show impaired B cell development but functional allelic exclusion of the IgH locus." J Immunol **168**(12): 6286-6293.

Su, T. T., B. Guo, B. Wei, J. Braun and D. J. Rawlings (2004). "Signaling in transitional type 2 B cells is critical for peripheral B-cell development." Immunol Rev **197**: 161-178.

Ta, V. B., M. J. de Bruijn, L. Matheson, M. Zoller, M. P. Bach, H. Wardemann, H. Jumaa, A. Corcoran and R. W. Hendriks (2012). "Highly restricted usage of Ig H chain VH14

family gene segments in Slp65-deficient pre-B cell leukemia in mice." J Immunol **189**(10): 4842-4851.

ten Boekel, E., F. Melchers and A. G. Rolink (1997). "Changes in the V(H) gene repertoire of developing precursor B lymphocytes in mouse bone marrow mediated by the pre-B cell receptor." Immunity **7**(3): 357-368.

Tsubata, T. and M. Reth (1990). "The products of pre-B cell-specific genes (lambda 5 and VpreB) and the immunoglobulin mu chain form a complex that is transported onto the cell surface." J Exp Med **172**(3): 973-976.

Vale, A. M., P. Kapoor, G. A. Skibinski, A. Elgavish, T. I. Mahmoud, C. Zemlin, M. Zemlin, P. D. Burrows, A. Nobrega, J. F. Kearney, D. E. Briles and H. W. Schroeder, Jr. (2013). "The link between antibodies to OxLDL and natural protection against pneumococci depends on D(H) gene conservation." J Exp Med **210**(5): 875-890.

Weinstein, J. A., N. Jiang, R. A. White, 3rd, D. S. Fisher and S. R. Quake (2009). "High-throughput sequencing of the zebrafish antibody repertoire." Science **324**(5928): 807-810.

Winkler, T. H., H. Fehr and J. R. Kalden (1992). "Analysis of immunoglobulin variable region genes from human IgG anti-DNA hybridomas." Eur J Immunol **22**(7): 1719-1728.

Xu, J. L. and M. M. Davis (2000). "Diversity in the CDR3 region of V(H) is sufficient for most antibody specificities." Immunity **13**(1): 37-45.

Figures
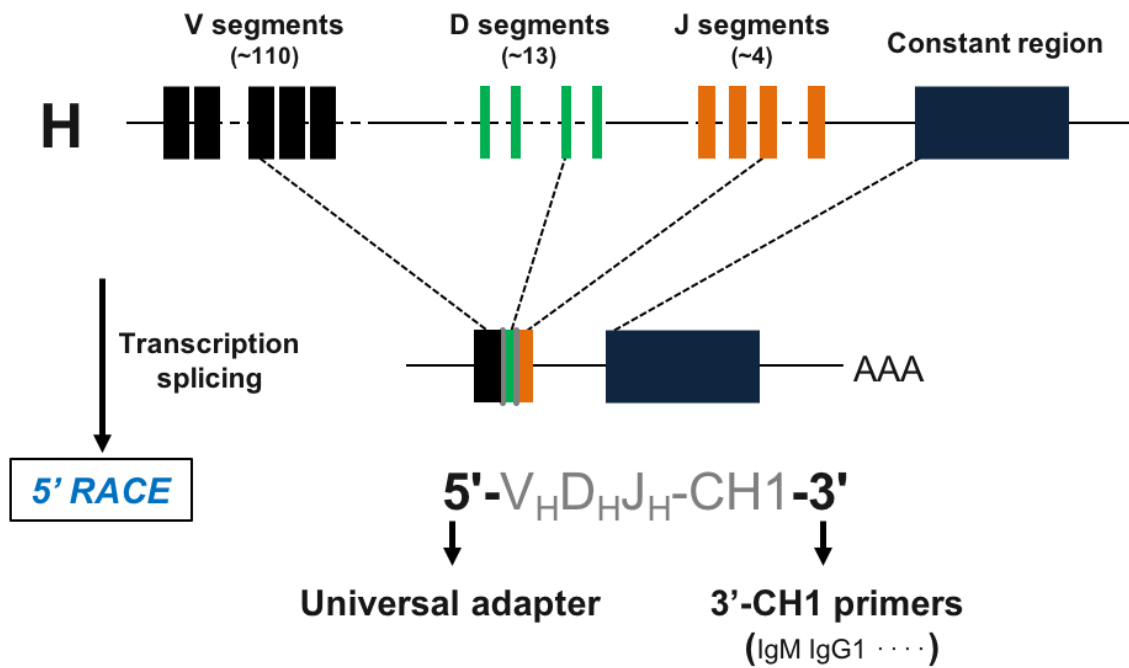
Figure 1. Scheme of sequencing strategy and visualization of antibody repertoire

Scheme of sequencing for V(D)J region: Spleens, bone marrow or sorted cells from naive mice were used to NGS analysis after the cDNA-synthesis and PCR-amplification of IgM, IgG1, IgG2c, Igκ or Igλ messages.
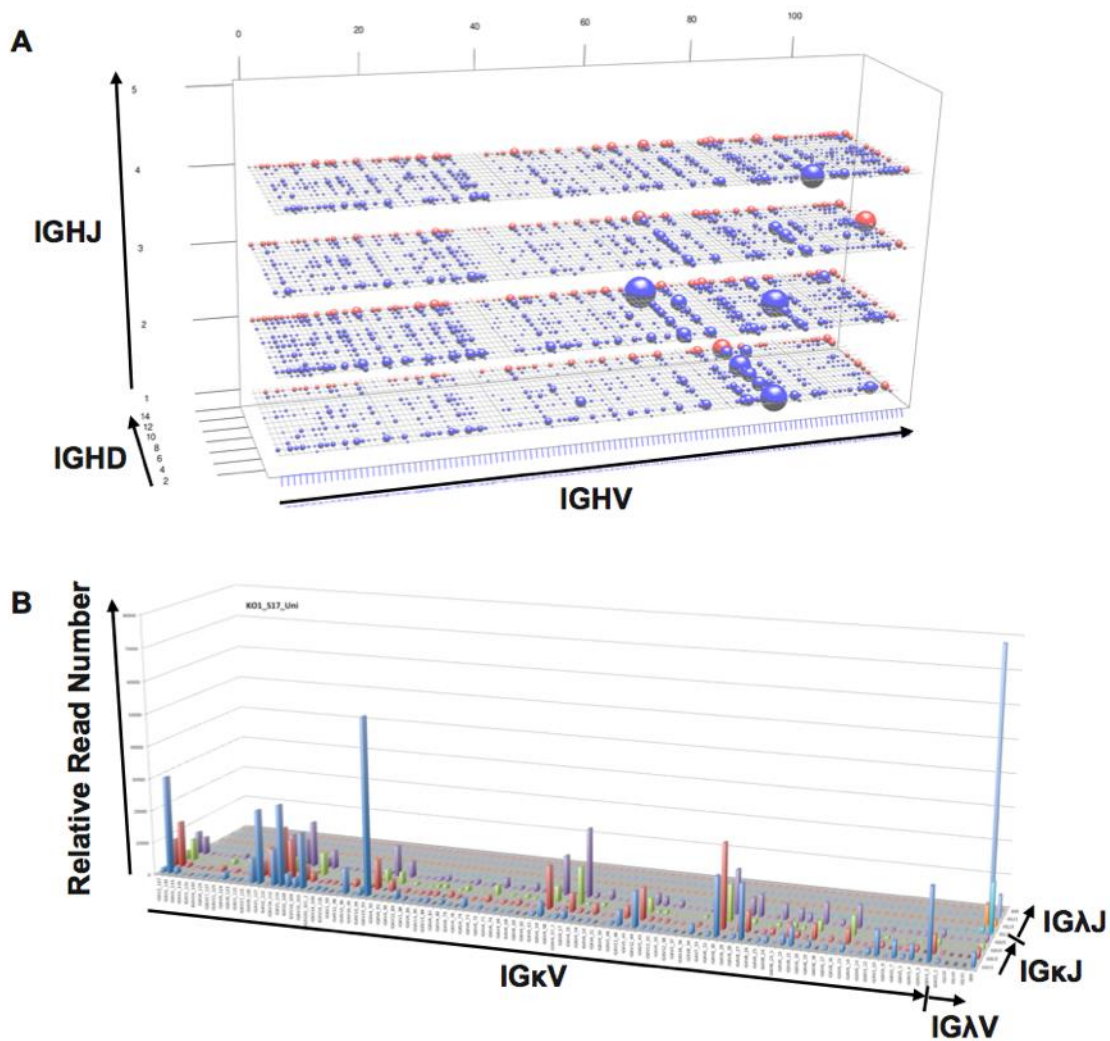
Figure 2. Visualization of the overall antibody-repertoire landscape

(A) IgH repertoires were visualized using an array on three-dimensional mesh, 3D-VDJ-plots. The x-axis represents 110 x IGHV genes, and the y-axis represents 12 x IGHD genes and z-axis represents 4 x IGHJ genes. The volume of each sphere represents the relative number of reads on each node. Red spheres: unannotated V, D, and J genes.
(B) IgL repertoires, visualized using an array on two-dimensional 2D-VJ-plots. The x-axis represents 101 x IGLVκ and 3 x IGLVλ genes, and the y-axis represents 4 x IGLJκ and 3 x IGLJλ genes. The length of each bar represents the relative number of reads on each node, and the unannotated V- and J-genes are represented on the far right.
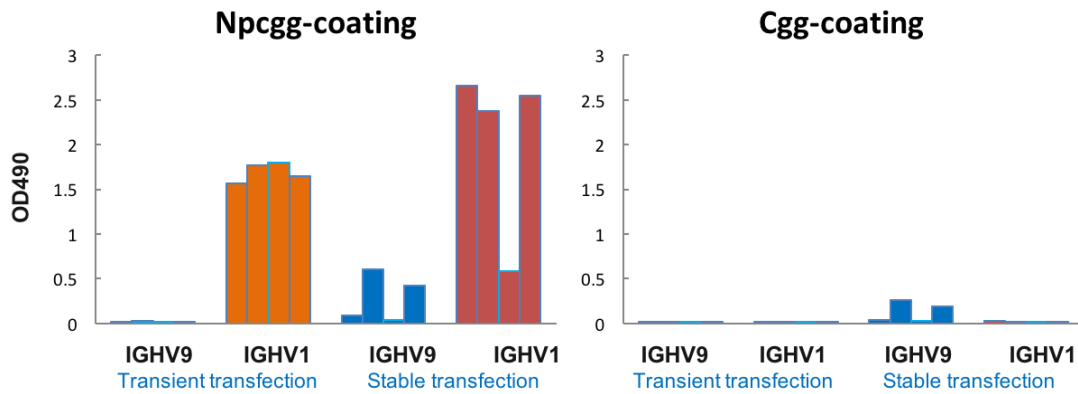
Figure 3. ELISA tests for binding to NP-CGG and CGG

The antibody genes, IGHV1 and IGHV9, were synthesized from the NGS reads and cloned into the expression vector in combination with λ1 LC. Antibodies were expressed in CHO cells and culture supernatants for both transient transfection and stable transfection were tested using ELISA for binding to NP-CGG and CGG.
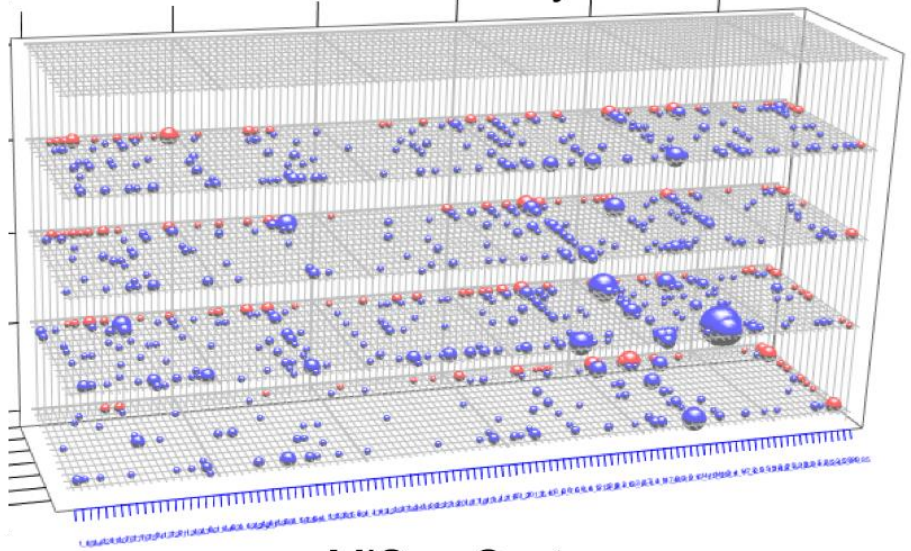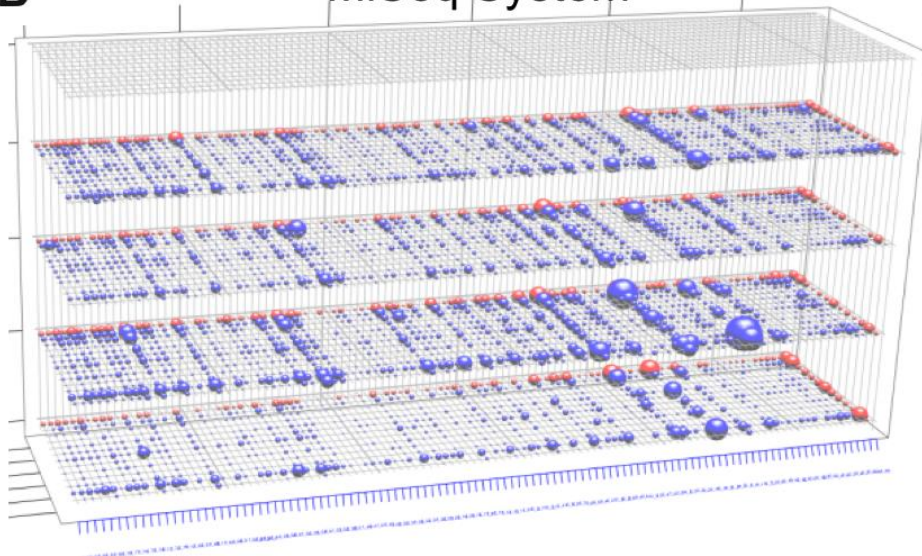
Figure 4. Comparison of Roche 454 system and MiSeq system

Spleen total RNA from the same WT individual mouse was purified and sequenced by Roche 454 system (A) and MiSeq system (B). Collected reads were arrayed on 3D-VDJ-plots.
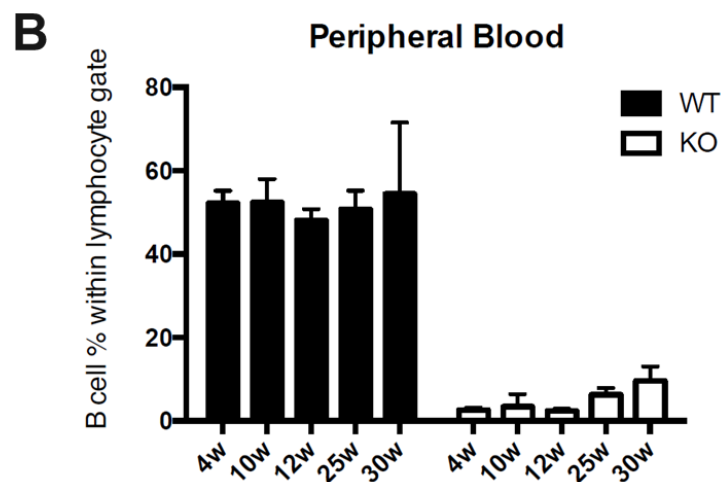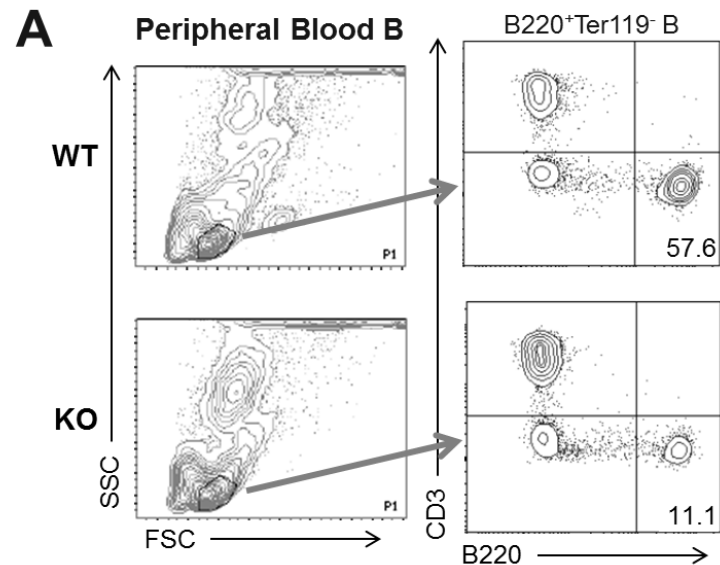
Figure 5. Leaky B cells in the peripheral blood of WT and KO ($\lambda 5^{-/-}$) mice

(A) Phenotypic analysis of peripheral blood B cells from WT and $\lambda 5^{-/-}$ mice. Peripheral B cells from littermates were collected from 4- to 30-week-old animals and analyzed by flow cytometry for B and T lymphocytes. Profiles in 30-week-old animals. (B) Percentages of B220$^+$ B cells within the lymphocyte gate at the indicated ages (n = 4 (WT, 4w); n = 5 (KO, 4w); n = 3 (WT, 10w); n = 4 (KO, 10w); n = 4 (WT, 12w); n = 4 (KO, 12w); n = 3 (WT, 25w); n = 4 (KO, 25w); n = 3 (WT, 30w); n = 4 (KO, 30w).
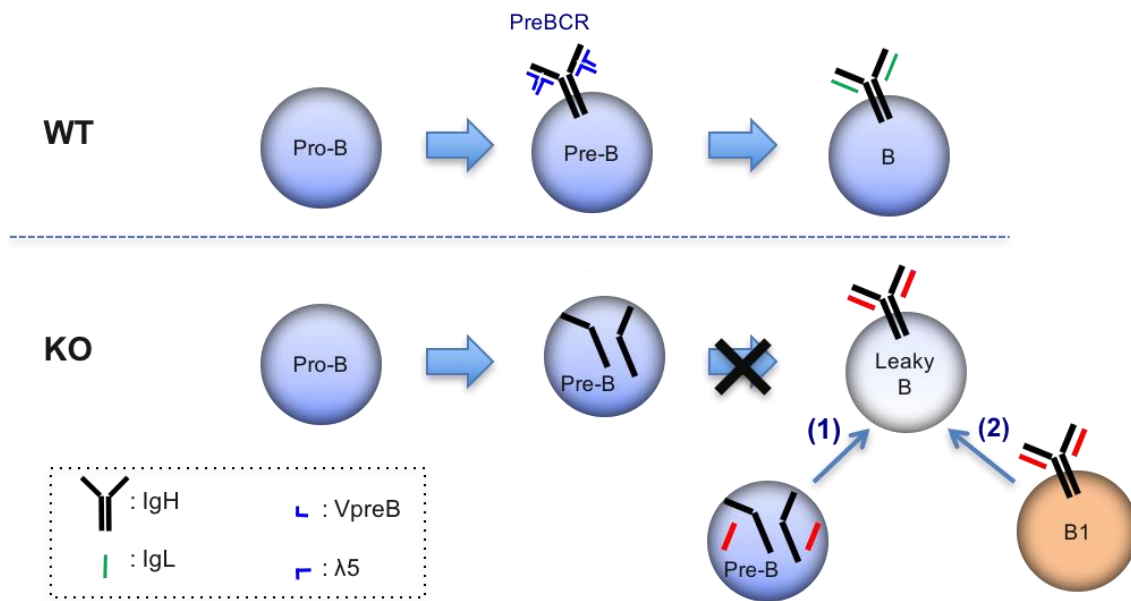
Figure 6. Hypothetical pathwayss for the leaky B cell generation.
Two potential pathways for leaky B cell generation in $\lambda 5^{-/-}$ mice, versus WT B cell development. Pathway (1) proposes that a minority of pre-B cells undergo spontaneous LC gene rearrangements, in the absence of pre-BCR. Pathway (2) proposes that leaky B cells originate from B1 cells, derived from the fetal liver and/or peritoneal cavity.
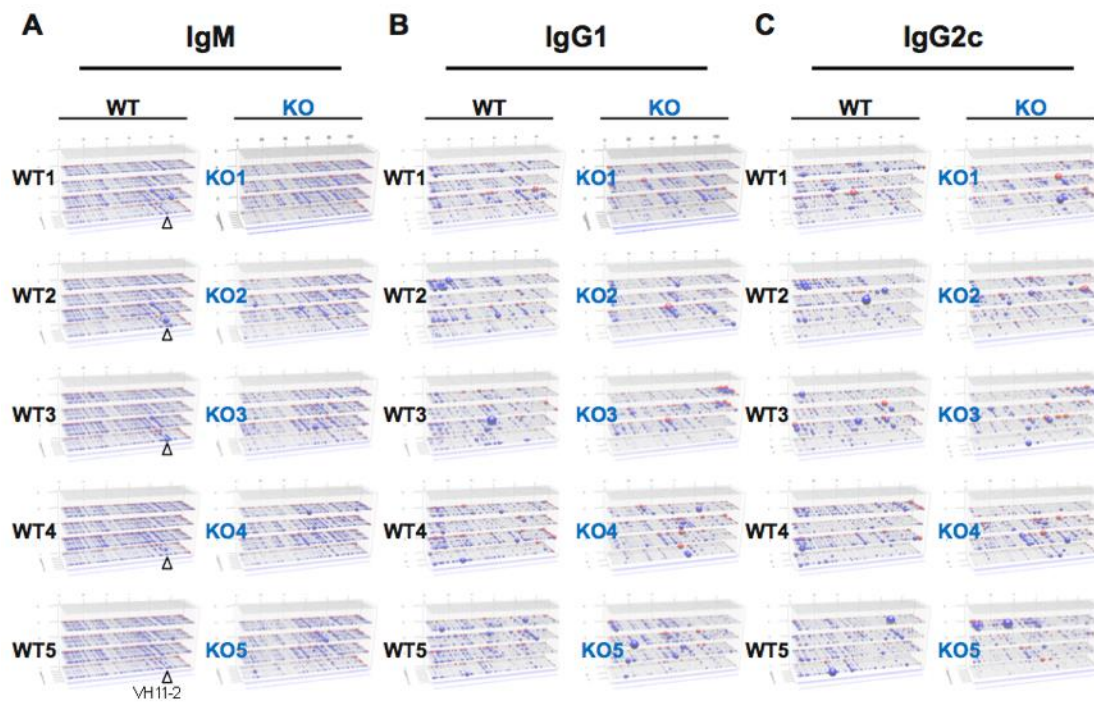
Figure 7. Repertoire analyses of WT and λ5⁻/⁻ (KO) spleen B cells, visualized using 3D-VDJ-plots

Spleen B cell repertoires for IgM (A), IgG1 (B), and IgG2c (C) from five WT and five λ5⁻/⁻ littermates were analyzed using NGS-based class-specific VDJ sequence analysis. Each group of WT mice (left) and λ5⁻/⁻ mice (right) is shown.
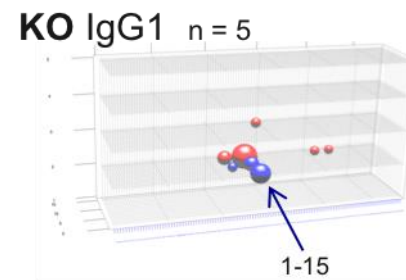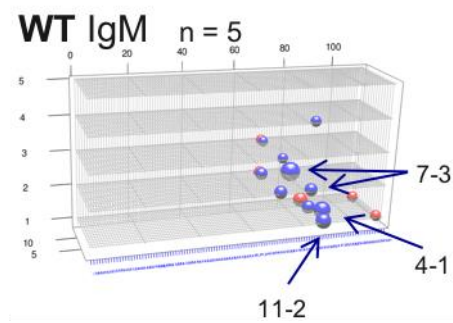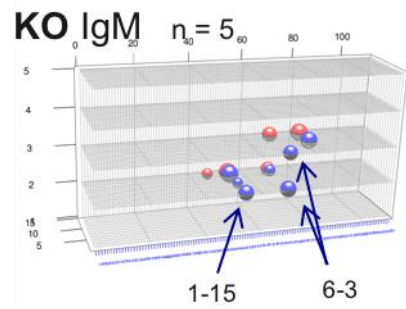
Figure 8. The common components in VDJ profiles of WT mice and λ5$^{-/-}$ (KO) mice were different

Visualization of the common components on the 3D-VDJ-plots of holistic repertoires of IgM, IgG1 in the spleen of five WT and five λ5$^{-/-}$ mice. Major repertoires in WT IgM (IGHV11-2, 4-1, and 7-3), λ5$^{-/-}$ mice IgM (IGHV1-15, and 6-3) and IgG1 (IGHV1-15) are indicated by arrows.

67
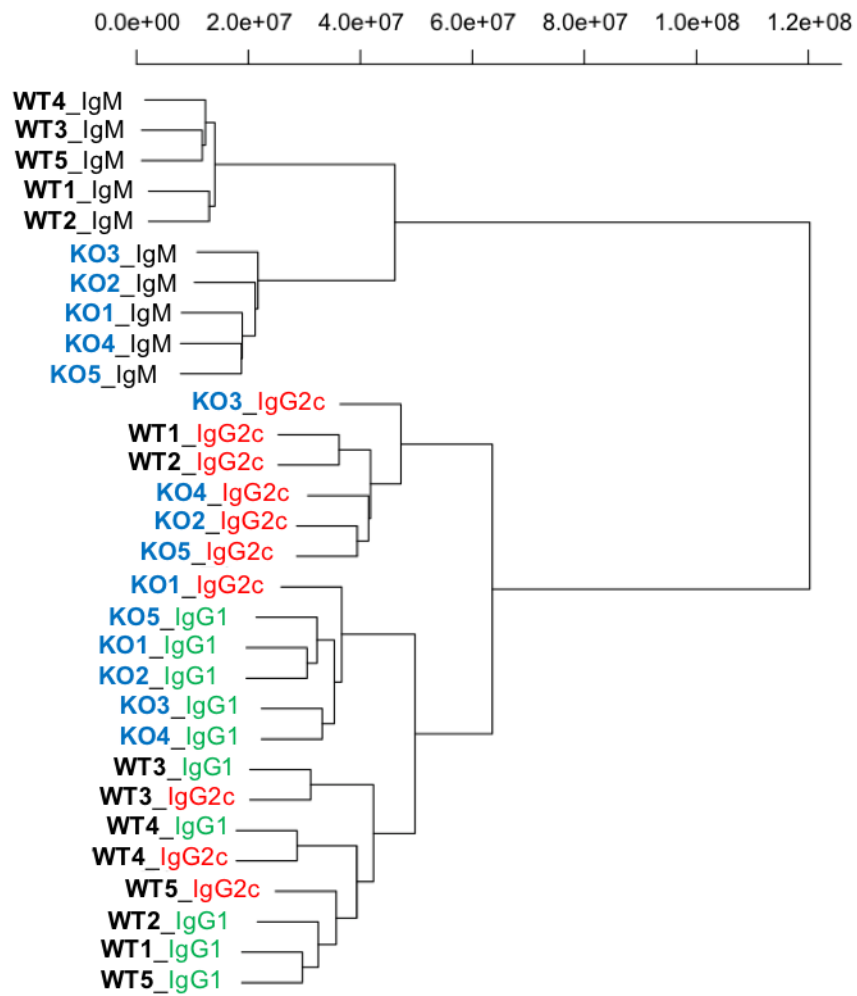
Figure 9. Phylogenetic tree representation of antibody repertoires of the IGH subclass.

Cluster analysis of VDJ-usage in the IGH subclass of genes from five WT (WT1~5) and five $\lambda 5^{-/-}$ (KO1~5) spleens.
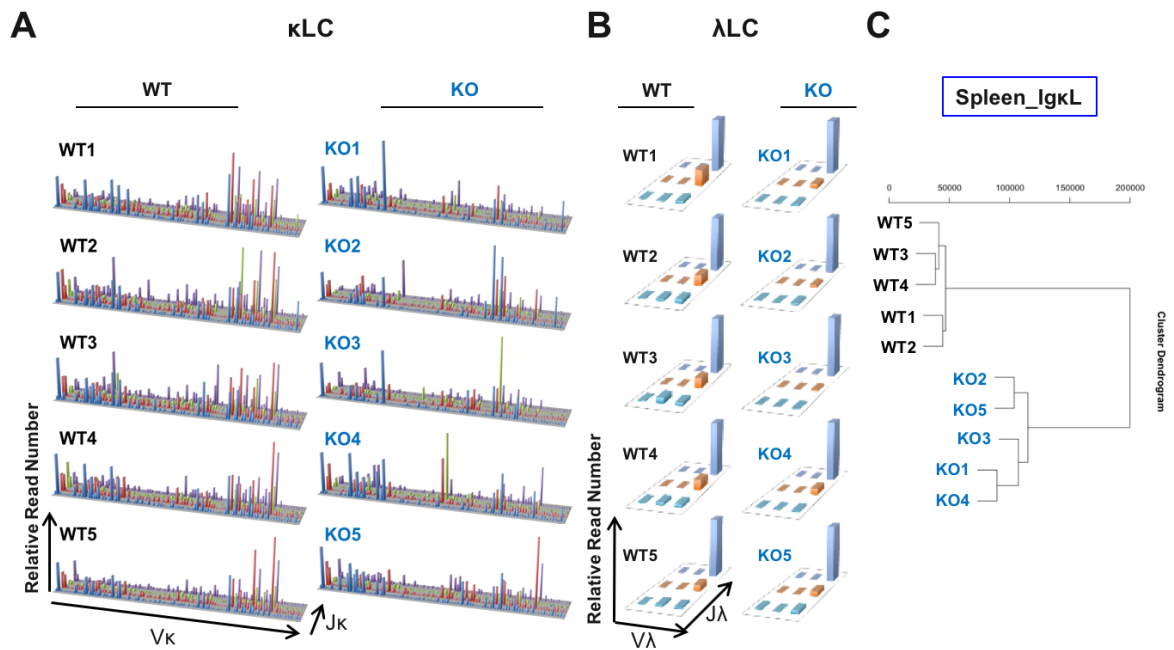
Figure 10. Cluster analysis of VJ$_\kappa$ usage profiles.

(A) The VJ distribution of IgκL in WT mice (Left) and $\lambda 5^{-/-}$ mice (Right). X-axis represents 101 V$_\kappa$ gene segments and Y-axis represents 4 J$_\kappa$ gene segments. (B) The VJ distribution of IgλL in WT mice (Left) and $\lambda 5^{-/-}$ mice (Right). X-axis shows 3 active V$_\lambda$ gene segments and Y-axis shows 3 J$_\lambda$ gene segments. (C) The cluster analysis of VJ$_\kappa$ usage profiles were performed for WT mice (n=5) and $\lambda 5^{-/-}$ mice (n=5). The 3D-VDJ-plots of the same samples were represented in Figure 7.
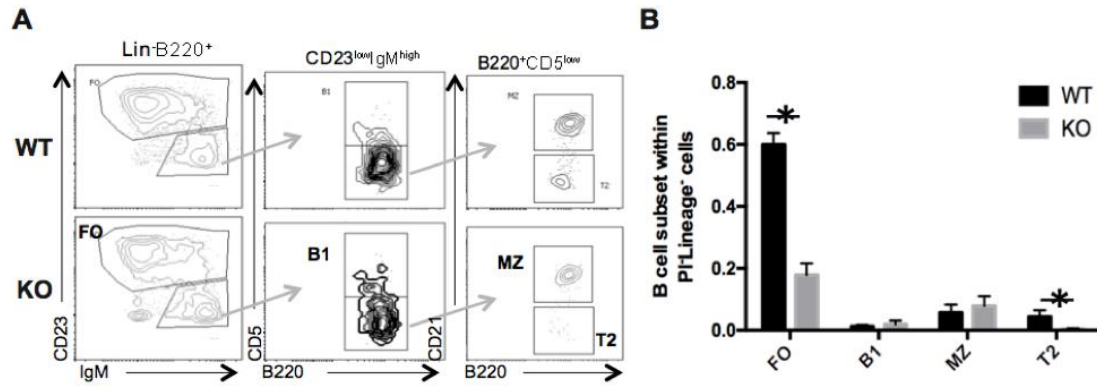
Figure 11. Cell sorting and characterization of spleen B cell subpopulations in WT and λ5$^{-/-}$ (KO) mice.

(A) Spleen B cells from five pooled WT versus KO mice were sorted into FO, T2, MZ, and B1 subpopulations. (B) Comparison of frequencies of B cell subpopulations in WT and λ5$^{-/-}$ mice (∗ ; $p < 0.05$, Student's t-test.)
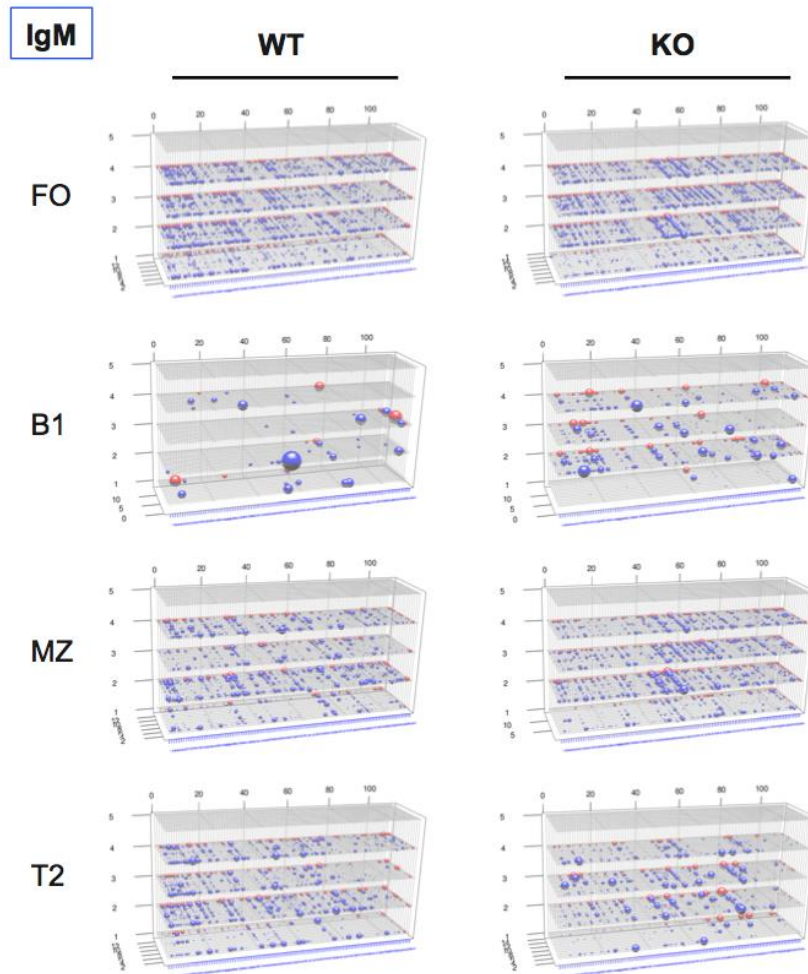
Figure 12. VDJ-usage profiles of the IgM repertoire for sorted B cell subpopulations.

Spleen B cells from 12-week-old mice (four mixed WT and four mixed λ5$^{-/-}$ (KO) littermates) were sorted using flow cytometry into FO, T2, MZ, and B1 subpopulations. The IgM VDJ-repertoires were compared for each subpopulation in WT (left) and λ5$^{-/-}$ mice (right).
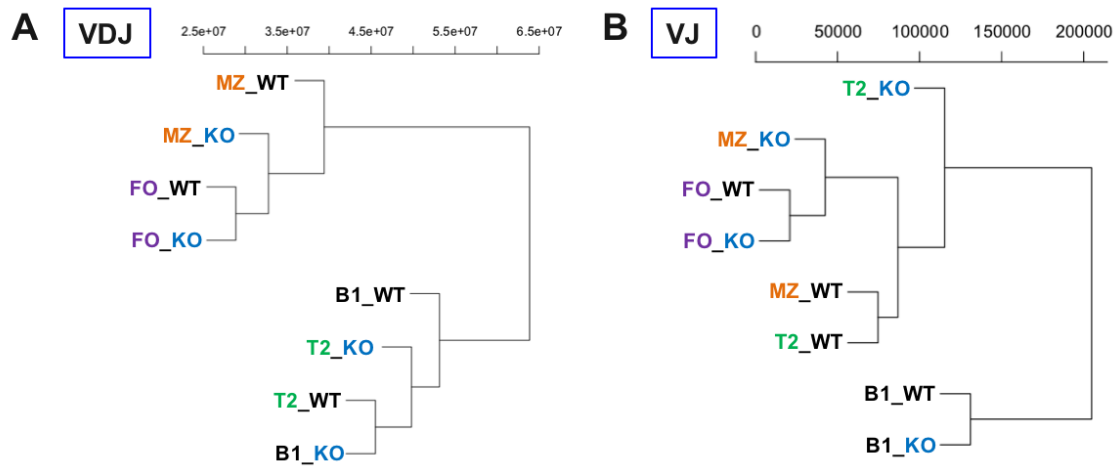
Figure 13. Cluster analysis for V(D)J genes of spleen B cell subpopulations

(A) Phylogenetic tree of IgH VDJ-usage distribution clusters in WT and λ5$^{-/-}$ mice. (B) Phylogenetic tree of IgL VJ-usage distribution clusters in WT and λ5$^{-/-}$ mice.
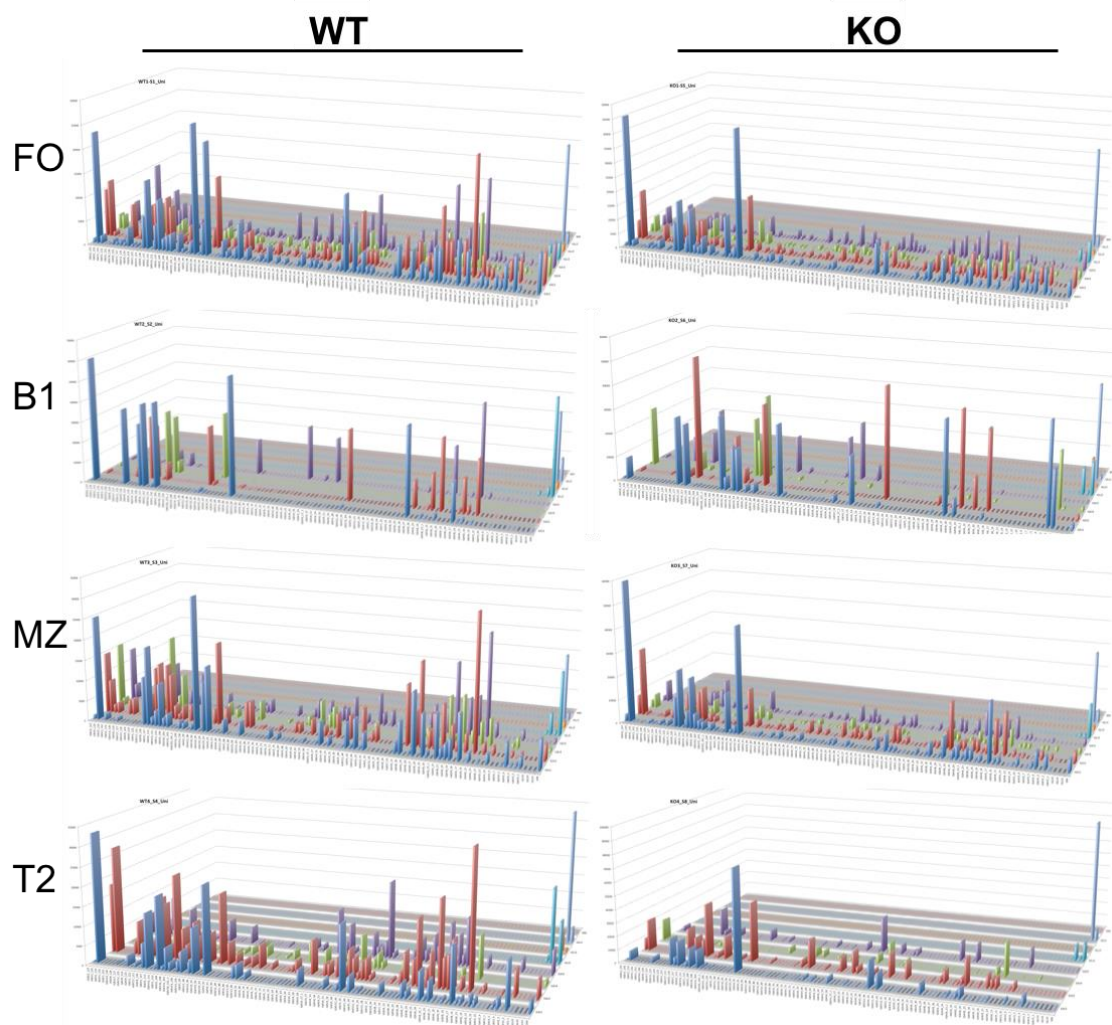
Figure 14. The VJ-usage profiles of IgL repertoire for sorted B cell subpopulations were represented by 2D-VJ-plots

Sorted B cell subpopulation were analyzed for the comparison of VJ-repertoires for each subpopulations form WT mice (Left) and $\lambda 5^{-/-}$ mice (Right).
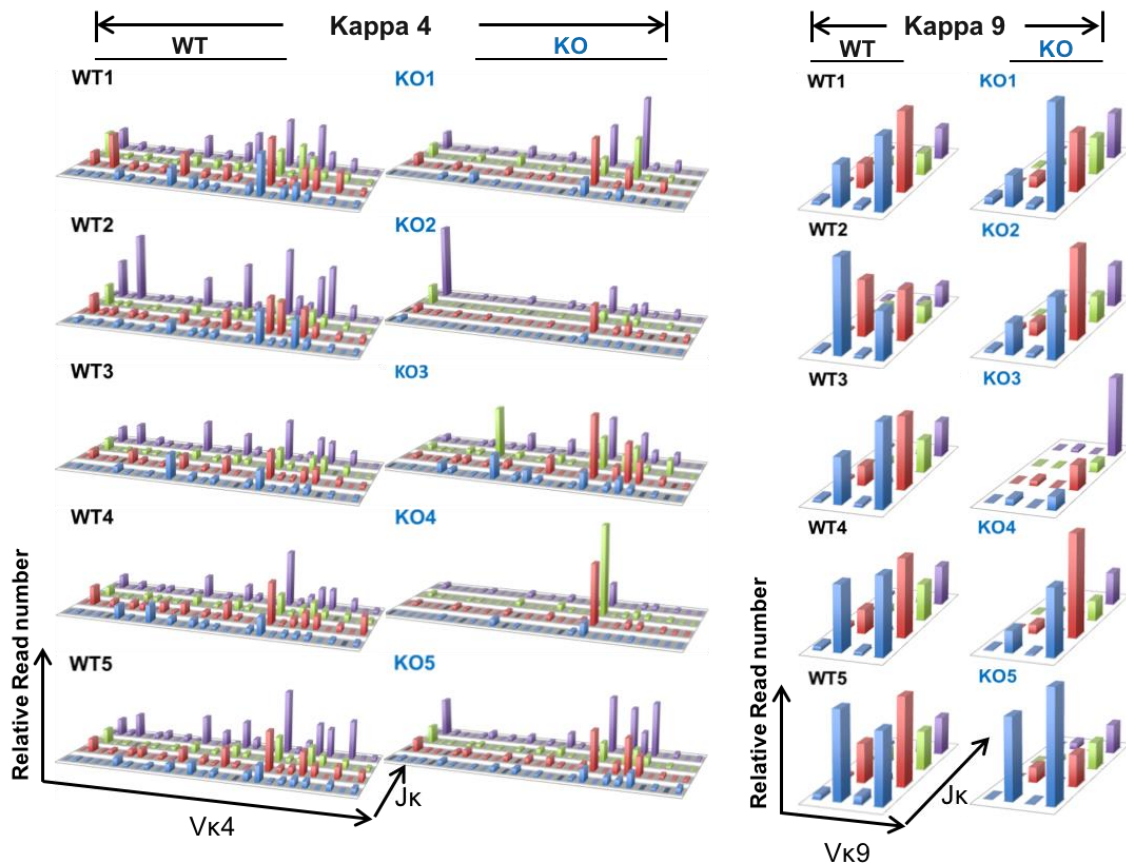
Figure 15. The NGS analysis of B1-ralated Ig-κ4 and Ig-κ9 showed similar pattern but decreased expression in λ5⁻/⁻ (KO) mice

Igκ4L (left) VJ distribution and (right) Igκ9L VJ distribution in WT mice and λ5⁻/⁻ mice. X-axis shows V_κ gene segments and Y-axis shows J_κ gene segments. The samples were same as the sample used in VDJ/VJ-repertoire analysis of spleen.
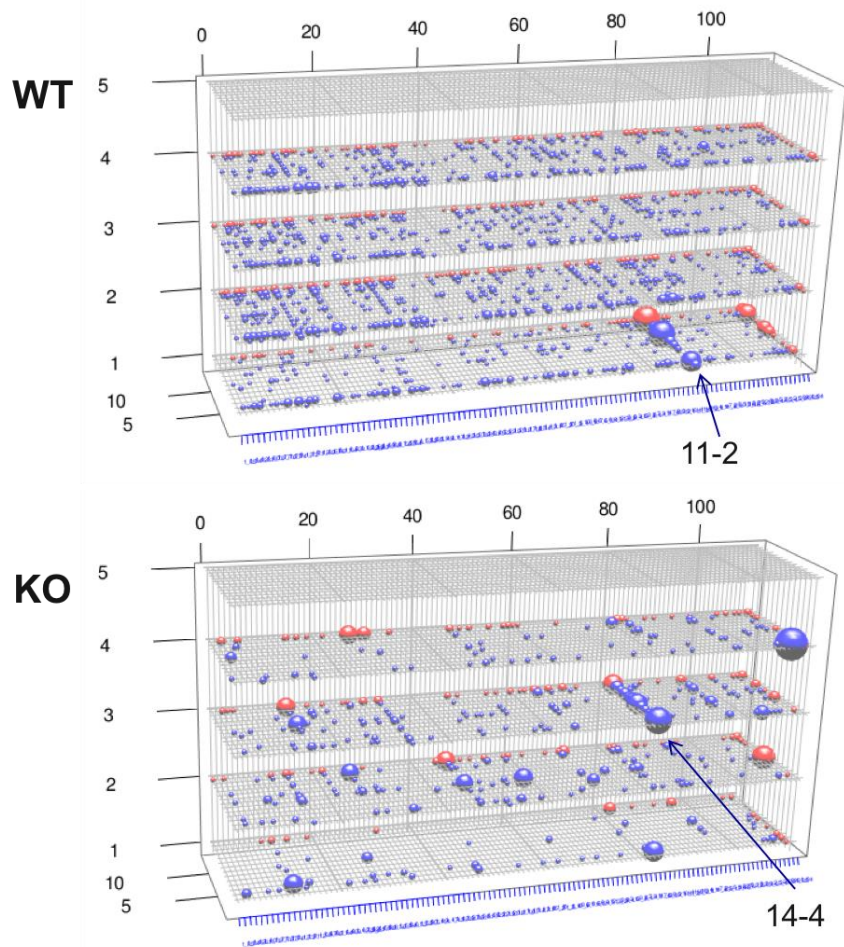
Figure 16. VDJ-3D-plot of total bone marrow cells in WT and λ5^{-/-} mice

Representative pattern of four WT and λ5^{-/-} littermates. The arrows indicate IGHV11-2 (in WT), and IGHV14-4 that was misread to IGHV11-2 (in λ5^{-/-}).

Figure 17. Bone marrow cells from five pooled WT and λ5$^{-/-}$ (KO) mice were analyzed by NGS for VDJ-usage distribution

(A) Amino acid sequences of CDR-H3 regions and frequencies in each mouse, listed in the order of their abundance; sequences containing Arg(s) in the middle are colored. (B) Frequency of CDR-H3 usage in WT and λ5$^{-/-}$ bone marrow cells. Top 20 CDR-H3 sequences in each mouse, shown as in (A) (bars represent SD).
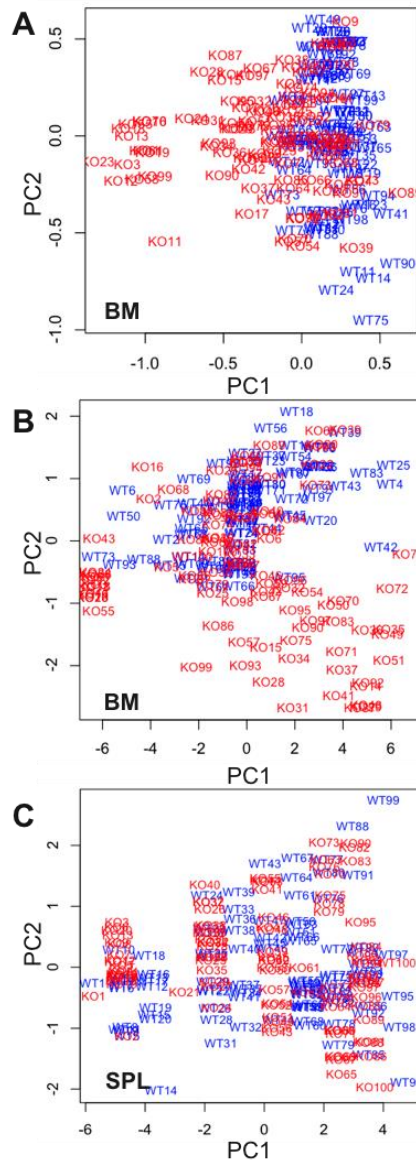
Figure 18. Amino acid descriptors calculated for the top 50 CDR-H3 amino acid sequences for each mouse and their discrepancy analyzed by Principal Component Analysis (PCA)

(A) Values for WT (WT, blue) and $\lambda 5^{-/-}$ (KO, red) mice, plotted on PC1 and PC2 axes (B) Amino acid descriptors, and the AaWtLpR index, calculated for the same sequence as in (A) and analyzed by PCA as in (A) (C) Amino acid descriptors, and the AaWtLpR index calculated for the top 50 CDR-H3 sequences in WT (blue) and $\lambda 5^{-/-}$ spleens (KO, red), analyzed by PCA as in (A)

	Comp.1	Comp.2	Comp.3	Comp.4	Comp.5	Comp.6	Comp.7	Comp.8	Comp.9	Comp.10
Helix/bend preference,	0.247	-0.271	-0.332	0.543	-0.194	0.184		0.590	0.195	
Side-chain size,		0.470	0.195	0.619		0.128	-0.270	-0.262		-0.434
Extended structure preference,	-0.594	-0.301	-0.322	0.368	0.184	0.117		-0.278	-0.239	0.368
Hydrophobicity,	-0.247				-0.376	-0.529	0.519	0.109	-0.350	-0.319
Double-bend preference,	0.175	-0.289	-0.330		0.484		0.252	-0.325	0.196	-0.577
Partial specific volume,	-0.218		-0.201	-0.210	-0.662	0.386		-0.325	0.380	-0.141
Flat extended preference,	-0.325	-0.483	0.667		0.105	0.300		0.209		-0.258
Occurrence in alpha region,	0.575	-0.393	0.254	0.193	-0.250			-0.450	-0.314	0.188
pK-C,		0.358	0.191	0.143	0.197	0.335	0.759		0.151	0.251
Surrounding hydrophobicity		-0.113	0.230	0.272		-0.546		-0.192	0.684	0.233

Figure 19. The Kidera Factor loadings of the PCA ananlysis in Figure 18A

A part of factor loadings of the PCA calculation is represented. The red figure shows the most predominant factor for separating WT and $\lambda 5^{-/-}$ (KO).

	Comp.1	Comp.2	Comp.3	Comp.4	Comp.5	Comp.6	Comp.7	Comp.8	Comp.9	Comp.10
#AAjLength	0.977				-0.11					
#AlaAbsLp					-0.106		0.71	-0.401	0.174	0.204
#CysAbsLp										
#AspAbsLp			0.631	-0.313	0.138	0.112	-0.239	-0.369	-0.432	
#GluAbsLp										
#PheAbsLp		0.185						0.306	0.164	-0.139
#GlyAbsLp		0.121	-0.357	-0.486	-0.424	0.543	-0.153	0.117		0.116
#HisAbsLp										
#IleAbsLp				0.104			-0.121			
#LysAbsLp										
#LeuAbsLp		-0.274	-0.136		0.141	-0.196	0.171	0.517	-0.588	0.228
#MetAbsLp							0.136	-0.269	-0.109	
#AsnAbsLp						0.151	0.262	0.202		-0.802
#ProAbsLp						-0.166	0.126			
#GlnAbsLp										
#ArgAbsLp		-0.585	-0.344	-0.103	0.472		-0.248	-0.283	0.201	-0.182
#SerAbsLp		0.312	-0.1	0.641	0.299	0.505			-0.126	0.183
#ThrAbsLp		-0.126		0.385	-0.517	-0.302	-0.392	-0.135		
#ValAbsLp			0.112	0.121	-0.235	-0.121				-0.103
#TrpAbsLp		-0.104	0.437		0.109			0.308	0.558	0.374
#TyrAbsLp	0.141	0.651	-0.256	-0.22	0.292	-0.461	-0.198		0.115	

Figure 20. The WtLpR factor loadings of PCA analysis in Figure 18B

The factors are the relative positional weight of twenty amino acids in the CDR-H3 loop. A part of factor loadings of the PCA is shown. The red figure, the relative position of Arg in the CDR-H3 loop, indicates the most predominant factor for separating WT and $\lambda5^{-/-}$ (KO).
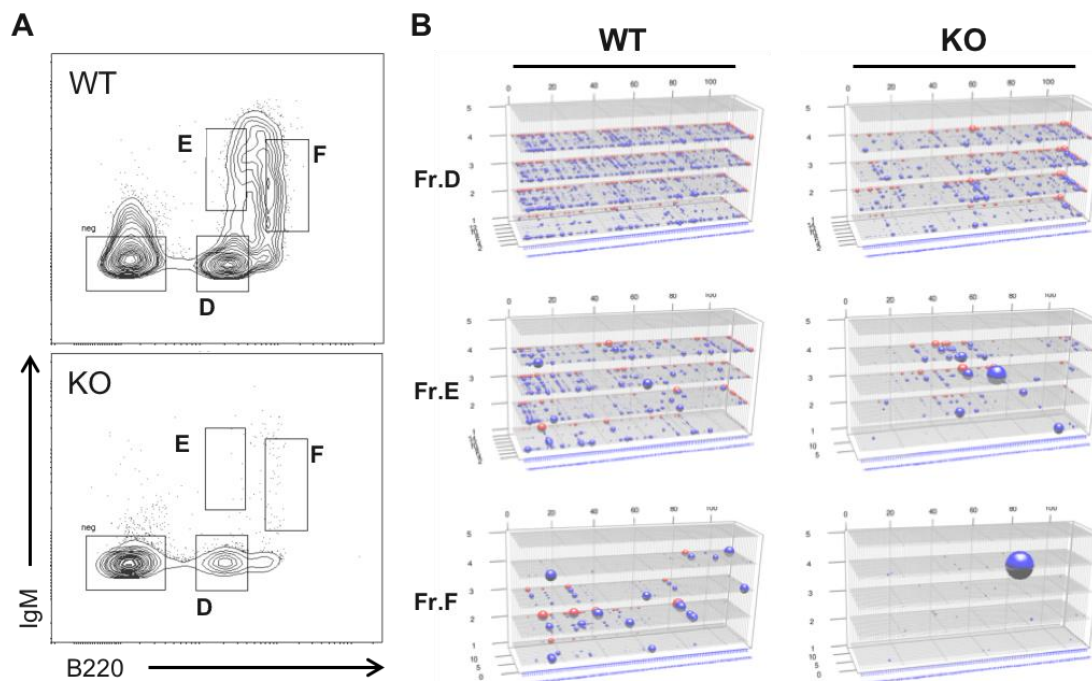
Figure 21. The VDJ-usage and CDR-H3 sequence profile of sorted bone marrow cells

(A) Bone marrow cells from four WT or four $\lambda5^{-/-}$ littermates were pooled and sorted into $B220^{lo}IgM^{-}$ (Fr. D), $B220^{lo}IgM^{+}$ (Fr. E) and $B220^{hi}IgM^{+}$ (Fr. F). The Fr. D contains Hardy's Fr. C and Fr. C'. (B) The NGS-analyses were performed for each cell fraction, and VDJ-usage profiles of IgM are represented by 3D-VDJ-plots.
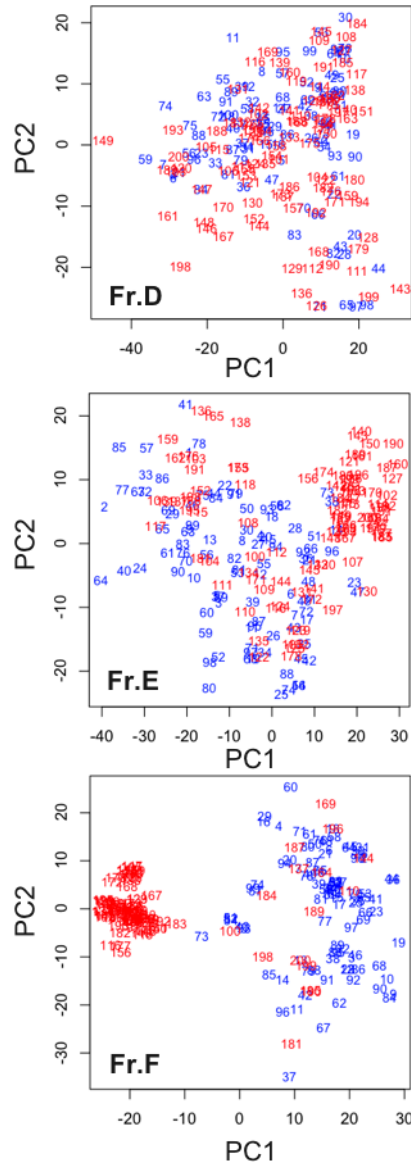
Figure 22. Primary component analysis (PCA) of CDR-H3 sequences from bone marrow B cell subpopulations

The amino acid sequences of CDR-H3 were deduced from IgBLAST outputs and the amino acid descriptors of each CDR-H3 sequence were calculated. The CDR-H3 sequences were sorted by their abundance ratio and the properties of top 100 sequences of WT (blue) and λ5$^{-/-}$ (red) were examined by the primary component analysis (PCA) of the Kidera Factors.
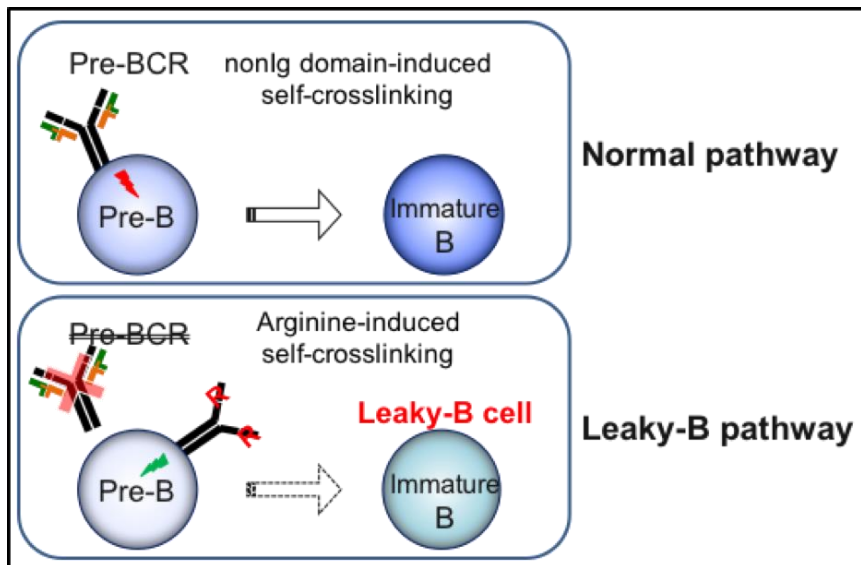
Figure 23. Model of leaky B cell generation pathway

Pre-BCR-mediated LC recombination is an important checkpoint during early development in WT mice (upper panel). In λ5$^{-/-}$ mice, the Arg(s) distribution at the center of CDR-H3 loop are elevated, suggesting that Arg(s)-induced self-crosslinking might activate signaling for cell differentiator in pre-B stage to give rise leaky B cells (bottom panel).
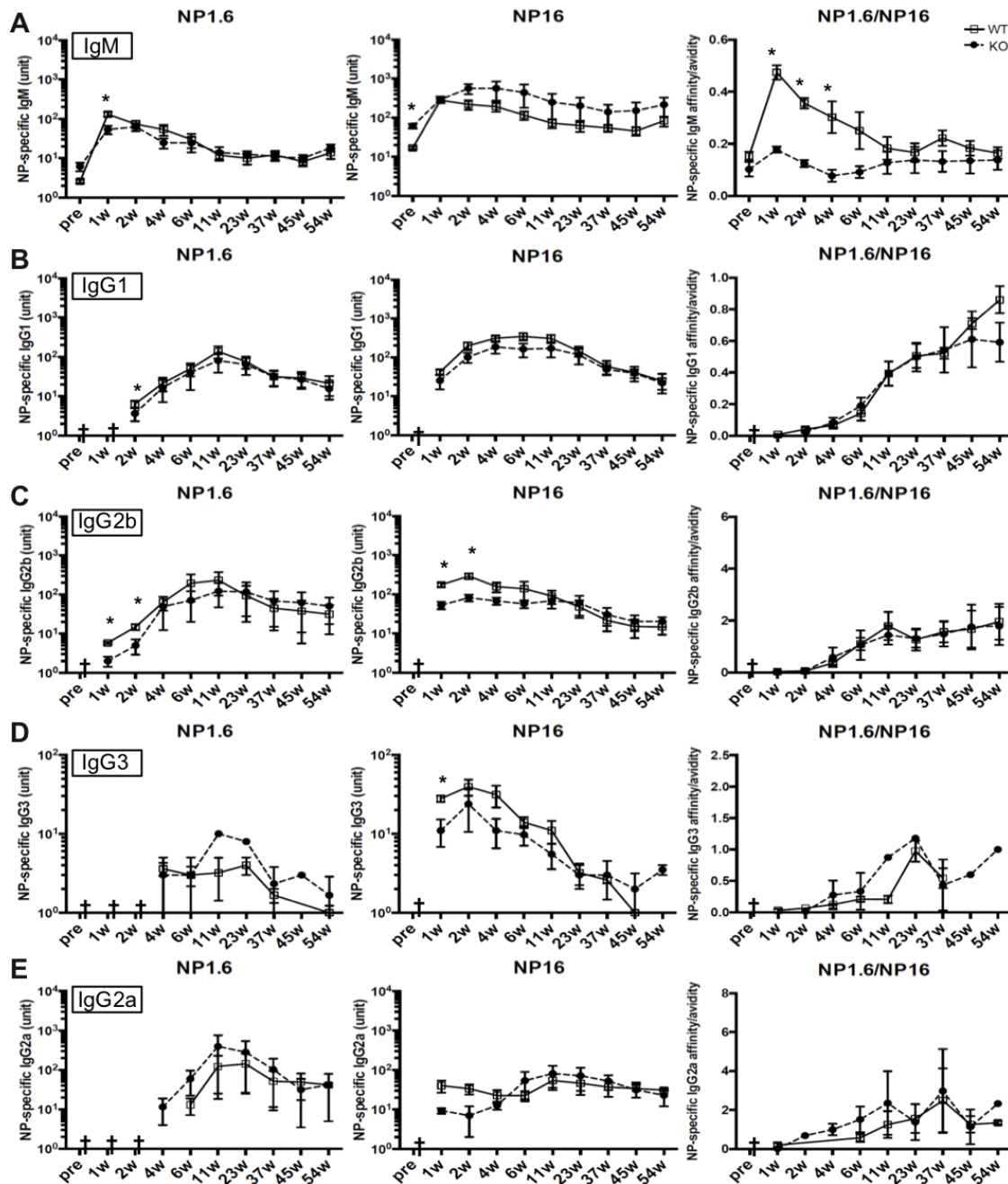
Figure 24. Primary immunization with NP showed significant difference at an early stage

Littermates were immunized with NP-CGG in alum. The titers of serum IgM (A), IgG1 (B), IgG2b (C), IgG3 (D) and IgG2a (E) antibodies against NP-BSA were measured in an ELISA. Antibody titers are expressed in terms of units derived from a panel of reference monoclonal NP-specific antibodies. High affinity (NP1.6) and total affinity (NP16) are shown. Affinity ratios were calculated for high affinity (NP1.6/NP16). Statistical significance was tested using Student's t-test (n=5 (WT), n=5 (KO)).
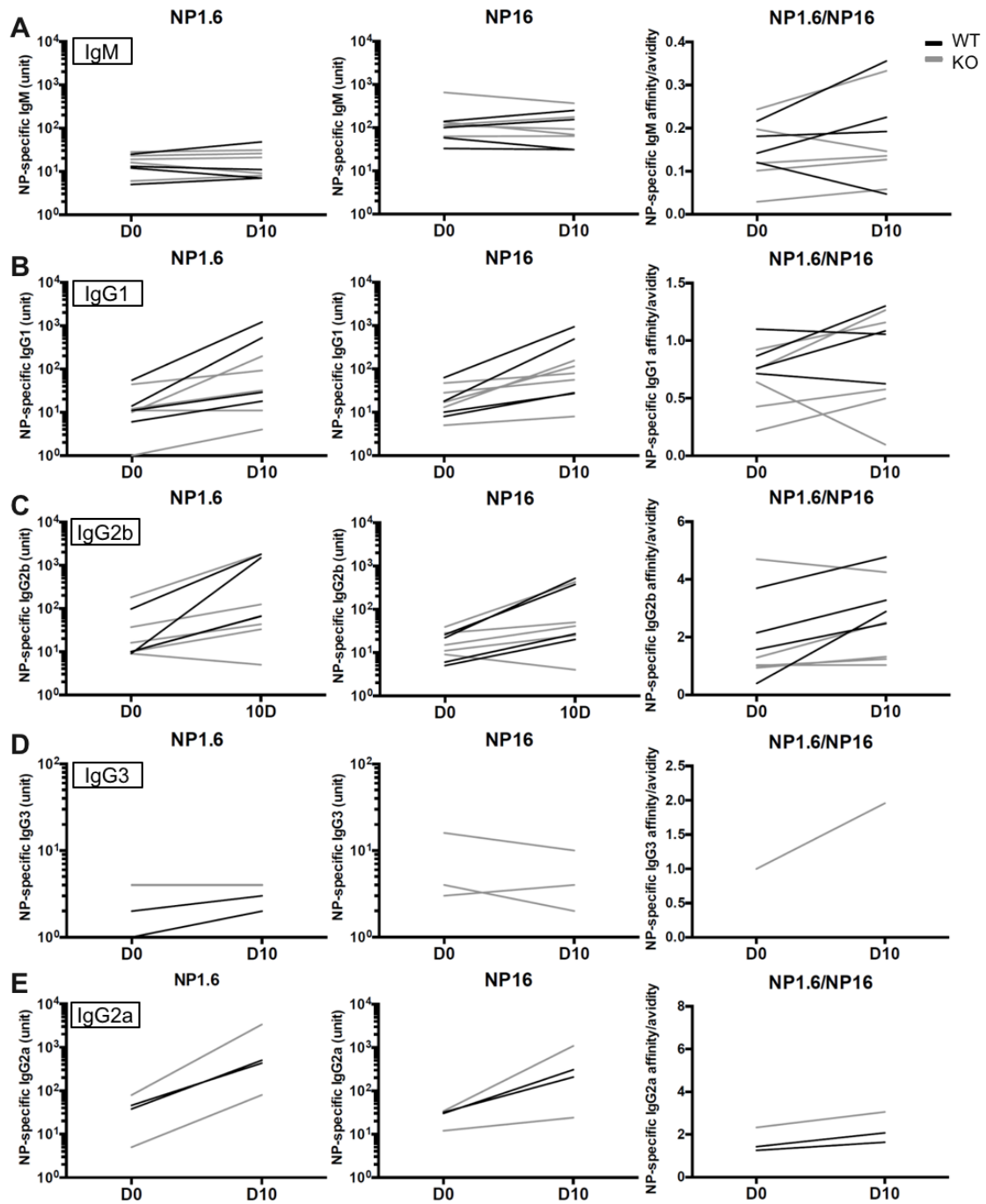
Figure 25. The secondary antibody response showed no significant differences between WT mice and λ5$^{-/-}$ mice

Littermates received primary immunization were boost immunized 57 weeks later. Serum titers of anti-NP antibodies were measured in an ELISA. The changes in NP-specific serum antibody titer in individual mice are plotted on a line graph.
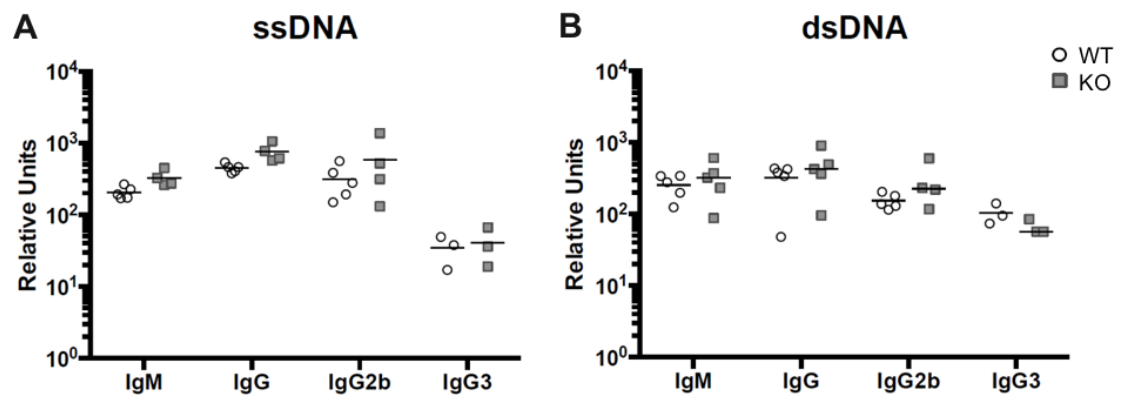
Figure 26. Slight elevated levels of antibodies against ssDNA and dsDNA in λ5$^{-/-}$ mice

The relative binding capacity of sera antibodies to ssDNA (A) or dsDNA (B) was determined by ELISA. Serum from MRLlpr-lpr mice was used as a positive control. Statistical significance was tested using Student's t-test (n=5 (WT), n=5 (KO)).